Neogene and Quaternary tectonics of the Eastern Sierras Pampeanas, Argentina: Active intraplate deformation inboard of flat-slab subduction

T. Richardson,[1] K. D. Ridgway,[1] H. Gilbert,[1] R. Martino,[2] E. Enkelmann,[3] M. Anderson,[4] and P. Alvarado[5]

Received 5 August 2012; revised 16 May 2013; accepted 22 May 2013.

[1] The ranges of the Eastern Sierras Pampeanas are located >600 km east of the Andean Cordillera in central Argentina and have been interpreted to be a response to shortening related to flat-slab subduction of the Nazca plate. Uplift of the ranges has been broadly documented to occur during Neogene time, but many questions remain regarding the timing and style of deformation, and the subsurface structural configuration. In this study, we address these unknowns with observations at multiple scales, integrate our results into a tectonic model for the area, and discuss how our structural interpretation fits with more regional tectonic models. Our major findings are: (1) The range-bounding faults thrust late Proterozoic to Cambrian schist and gneiss over poorly dated Pliocene to Pleistocene alluvial strata. The timing of fault displacement and age of footwall strata suggest that deformation may have been active at least by Pliocene time. (2) Apatite and zircon (U-Th)/He thermochronometry exhibits cooling ages that range from Permian to Early Jurassic time and suggests that rock exhumation in the area is less than 2–3 km since that time. (3) Deploying a local seismic array allowed for locating seismicity and calculating receiver functions. These observations indicate that the Moho lies at a depth of 37 km and that a midcrustal discontinuity appears to correspond to a detachment zone between 15 and 20 km depth and aligns with a plane of seismicity. In our tectonic model, the craton appears to act as a rigid backstop to the eastward propagation of stresses from the shallowly subducting slab. Deformation then propagates back to the west via westward-verging faults along a midcrustal detachment.

Citation: Richardson, T., K. D. Ridgway, H. Gilbert, R. Martino, E. Enkelmann, M. Anderson, and P. Alvarado (2013), Neogene and Quaternary tectonics of the Eastern Sierras Pampeanas, Argentina: Active intraplate deformation inboard of flat-slab subduction, *Tectonics*, *32*, doi:10.1002/tect.20054.

1. Introduction

[2] The western margin of South America has been a convergent plate boundary since late Mesozoic time, resulting in the development of the Andean Cordillera [*Ramos and Aleman*, 2000]. During this time of convergence, flat-slab subduction of segments of the downgoing Nazca plate has resulted in spatial and temporal changes in the style of deformation of the overriding South American plate [*Jordan et al*., 1983; *Ramos et al*., 2004]. During active flat-slab subduction, the continental plate is extensively shortened, and deformation propagates inboard away from the margin, leading to the formation of basement-involved uplifts, or arches, in and beyond the foreland basin [*Ramos*, 2009]. The Sierras Pampeanas of central Argentina between 29° and 33°S (Figure 1) are considered an example of active thick-skinned crustal deformation that is related to flattening of the Nazca plate since ~15 Ma [*Jordan and Allmendinger*, 1986; *Kay and Abbruzzi*, 1996; *Ramos et al*., 2002]. The Eastern Sierras Pampeanas are located more than 600 km from the plate margin and are considered the easternmost expression of crustal deformation (Figure 1).

[3] Several groups of ranges comprise the Eastern Sierras Pampeanas, including the Sierras de San Luis in the southwest and the Sierras de Córdoba in the east (Figure 2A). Our study focuses on observations made primarily within the Sierras de Córdoba, which includes the Sierra Norte, Sierra Chica, Sierra Grande, Sierra de Comechingones, and Sierra de Pocho, from east to west. These roughly N-S trending ranges have elevations up to ~2 km and are bounded

[1]Department of Earth and Atmospheric Sciences, Purdue University, West Lafayette, Indiana, USA.
[2]Departamento de Geología Básica, Universidad Nacional de Córdoba, Córdoba, Argentina.
[3]Department of Geology, University of Cincinnati, Ohio, USA.
[4]Department of Geology, Colorado College, Colorado Springs, Colorado, USA.
[5]Departamento de Geofísica y Astronomia, Universidad Nacional de San Juan, Rivadavia, San Juan, Argentina.

Corresponding author: K. D. Ridgway, Department of Earth and Atmospheric Sciences, Purdue University, 550 Stadium Mall Drive, West Lafayette, IN 47907-2051, USA. (ridge@purdue.edu)

0278-7407/13/10.1002/tect.20054

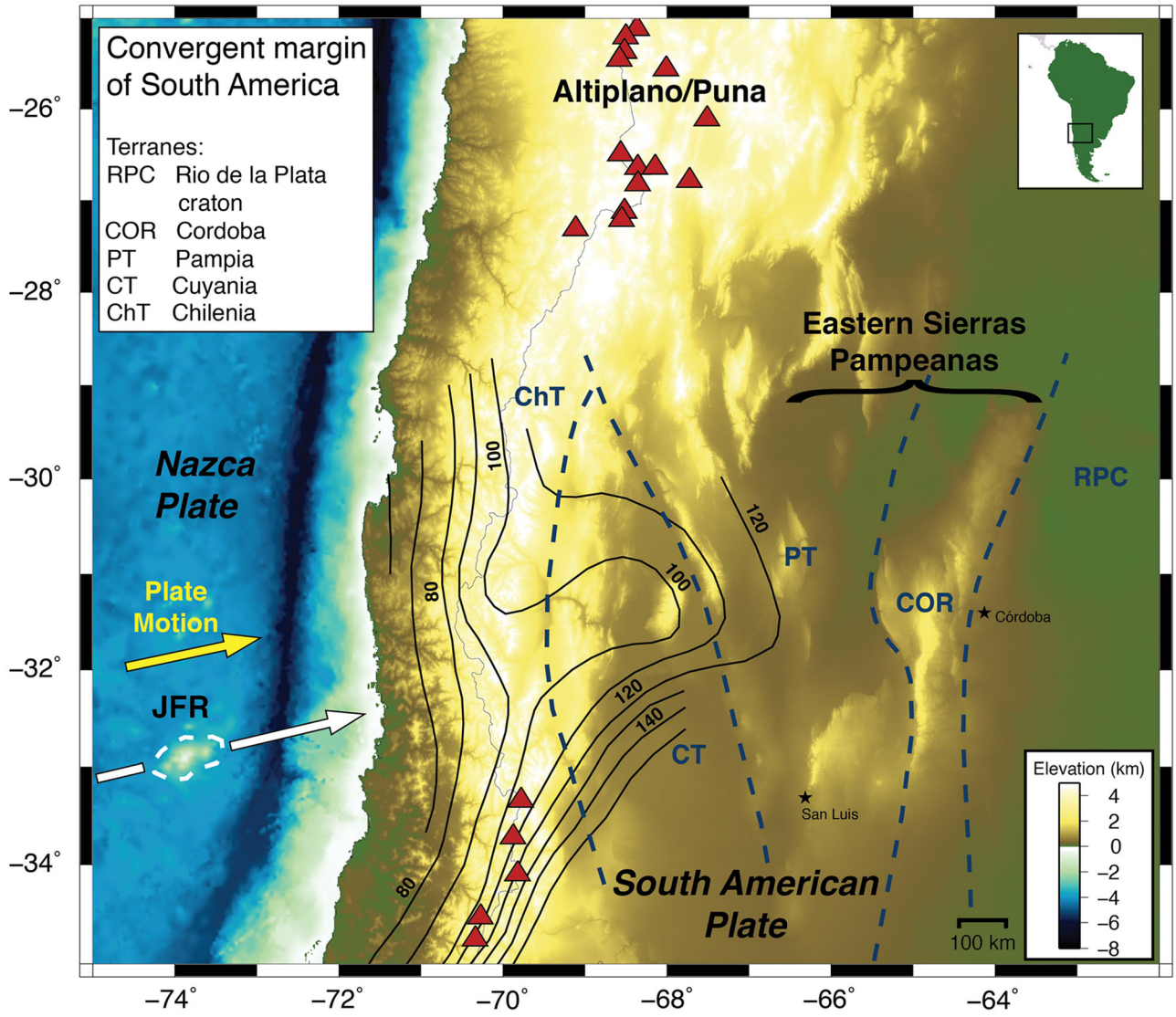

Figure 1. Regional shaded relief map of central Chile and Argentina along the western convergent margin of South America, as indicated by map inset (modified from *Alvarado et al*. [2009]). The surface expression of the Juan Fernandez Ridge (JFR) on the Nazca plate is outlined in white with a white arrow indicating its projection beneath the South American plate. Black lines signify depth contours following the top of the subducted Nazca plate, which flattens at less than 100 km depth beneath the Andes and Western Sierras Pampeanas [from *Anderson et al*., 2007]. Blue dashed lines indicate the proposed locations of crustal terrane boundaries from *Ramos et al*. [2002]; the boundary along the eastern margin of the Córdoba terrane is refined from *Rapela et al*. [2007] using results from this study. A black bracket bounds the E-W extent of the study area in the Eastern Sierras Pampenas and the location of Figure 2. Black stars indicate the location of major cities in the Eastern Sierras Pampeanas. Red triangles show the location of the active volcanic arc [*Stern*, 2004], and a yellow arrow indicates the direction of convergence of the Nazca plate at a rate of 6.7 cm/yr and azimuth of 78° [*Vigny et al*., 2009].

predominantly along their western slopes by east-dipping reverse faults, resulting in an overall westward vergence of the ranges (Figure 2a and b) [*Jordan and Allmendinger*, 1986; *Ramos et al*., 2002]. In this study, we present a complete set of geological and geophysical observations, ranging from the surface to the depth of the Moho, to better understand the configuration of active crustal faults, timing of Neogene and Quaternary deformation, and amount of exhumation of the Eastern Sierras Pampeanas. Using insights gained from integrating these new data sets, we modify a previously published geologic cross section from the Andes to the craton to reflect our improved understanding of regional upper-plate crustal deformation related to flat-slab subduction.

2. Geologic Framework and Previous Studies

[4] The Eastern Sierras Pampeanas have had a long history of deformation. During early to middle Paleozoic time, east-

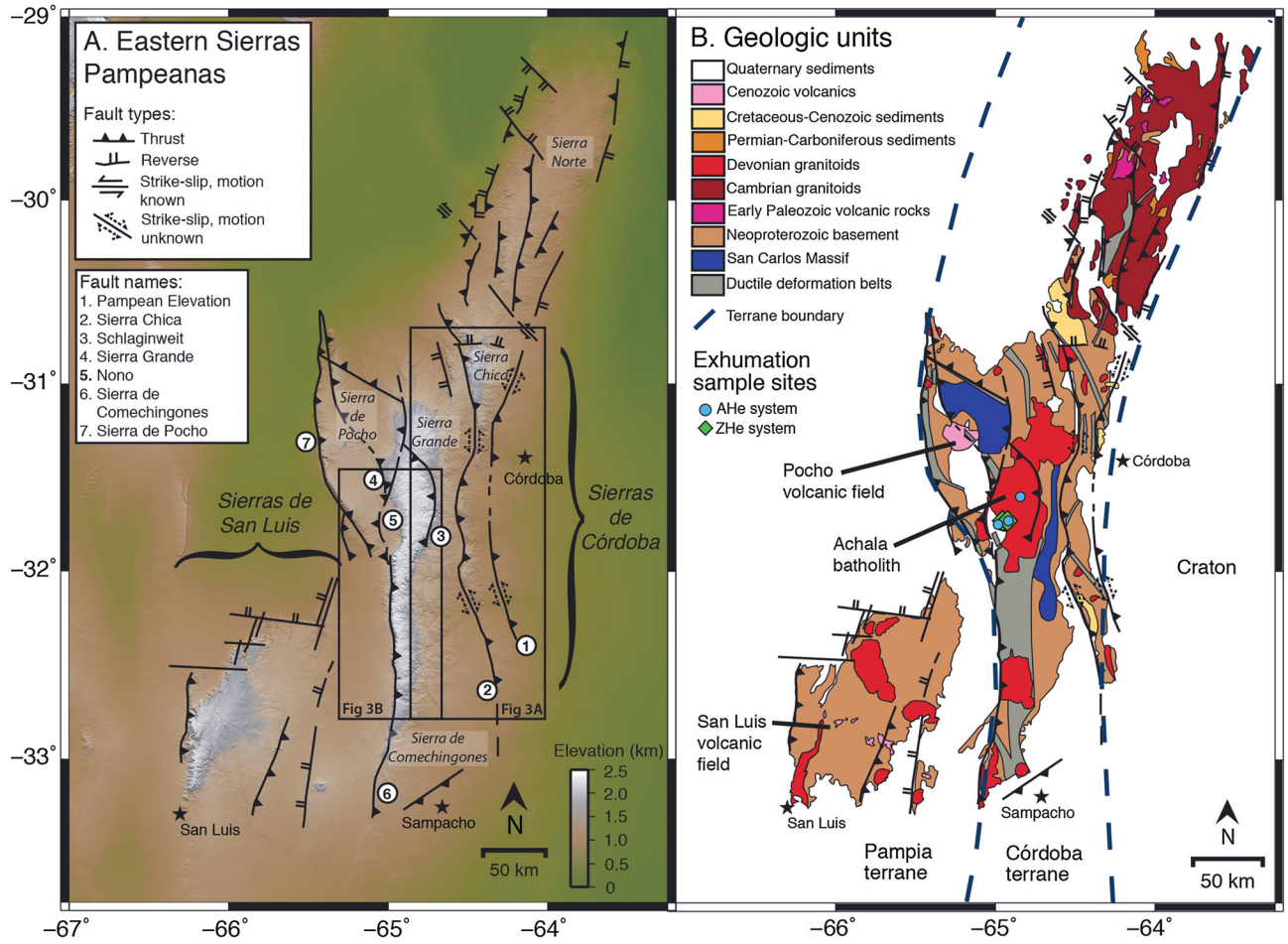

Figure 2. (a) Local shaded relief map of the Eastern Sierras Pampeanas showing the location of high topography, surface traces of main faults (based on updated map from *Martino* [2003]), and geographic divisions of the study area. The five principal ranges in the Sierras de Córdoba are individually labeled. Circled numbers label the primary faults addressed in this study, and dashed strike-slip symbols indicate uncertainty in the direction of motion. Two black squares outline the regions shown in A and B of Figure 3. (b) General geologic map of the region displaying the extent of dominant rock types in relation to faults. Dashed black lines indicate the locations of terrane boundaries. The location of exhumation samples in the Achala batholith are marked as blue circles for apatite samples and green diamonds for zircon samples. Arrows note the relative sense of shear motion across faults in Figures 2a and 2b, with dotted double-headed arrows indicating an uncertain sense of motion.

directed subduction along the western margin of South America resulted in the accretion of a series of terranes, including the Córdoba and Pampia terranes, onto the Rio de la Plata craton (Figure 1), which now compose the crust of the Eastern Sierras Pampeanas. East-directed subduction also resulted in the emplacement of Devonian batholiths within the Eastern Sierras Pampeanas (Figure 2b) [*Pankhurst et al*., 1998; *Rapela et al*., 1998, 2007; *Ramos and Aleman*, 2000; *Ramos*, 2009]. During Mesozoic time, extension of the western margin of South America formed rift basins along reactivated Paleozoic terrane boundaries [*Schmidt et al*., 1995; *Uliana et al*., 1989]. Andean deformation began in late Cretaceous time with subduction of the Farallon Plate. At ~10 Ma, a period of flat-slab subduction began at ~32°S likely in response to subduction of a series of seamounts known as the Juan Fernandez Ridge [*Yañez et al*., 2002]. The shallowing of the subducting plate caused magmatism and subsequent crustal deformation to propagate far into the interior of the continent [*Kay and Mpodozis*, 2002; *Ramos et al*., 2002; *Yáñez and Cembrano*, 2004] and thinned the mantle lithosphere by nearly 60% [*Kay and Abbruzzi*, 1996]. Volcanism above the leading edge of the flat slab reached the Eastern Sierras Pampeanas ~6 Ma, with the last activity occurring at the Pocho volcanic field between 6 and 5 Ma [*Gordillo and Linares*, 1981; *Kay and Gordillo*, 1994] and the San Luis volcanic field at about 1.9 Ma (Figure 2b) [*Ramos et al*., 1991; *Urbina et al*., 1997; *Kay and Mpodozis*, 2002; *Ramos et al*., 2002; *Löbens et al*., 2010].

[5] Across the entire Sierras Pampeanas, the timing of basement uplift has been interpreted to progress from north (~7 Ma) to south (~2.6 Ma) and west to east based on the stratigraphy of synorogenic strata and apatite fission track dating of basement rocks [*see review in Ramos et al*.,

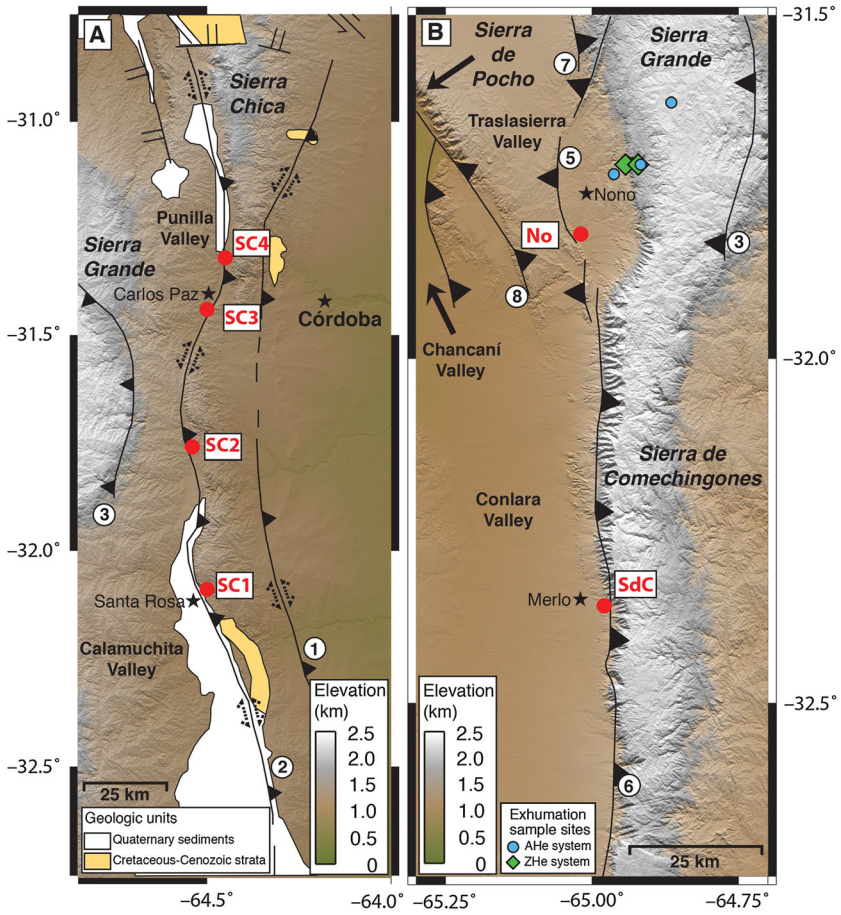

Figure 3. Shaded relief maps of the (a) Sierra Chica and (b) Sierra de Comechingones and Nono fault trace regions, with the positions of the maps outlined in Figure 2A. Labels indicate the location of major ranges, valleys, and towns. The location of fault exposures addressed in this study is indicated by red dots and labeled Sierra Chica (SC1-4), Nono (No), and Sierra de Comechingones (SdC). Figure 3A includes the mapped extent of Cretaceous and younger sediments along the Sierra Chica, as shown in Figure 2B. Circled numbers label the main faults according to the nomenclature of Figure 2A.

2002]. Previous range-specific studies have interpreted uplift of the western margin of the Sierras de Córdoba to begin between 6–5.5 Ma based on the relationship between faulting and distinct volcanic events in the Pocho volcanic field (Figure 2b) [*Jordan and Allmendinger*, 1986; *Kay and Gordillo*, 1994; *Ramos et al*., 2002]. The age of organic material in footwall strata of major reverse faults, and geomorphologic data from across the Sierras de Córdoba suggest that deformation has continued into the late Pleistocene to Holocene time [*Costa et al*., 2001, 2010; *Massabie et al*., 2003]. For the Sierra de San Luis and Sierra de Comechingones to the south (Figure 2A), the timing of uplift is poorly constrained, but is interpreted to be late Pliocene to Quaternary in age based on proximal synorogenic deposits (see references in review paper by *Ramos et al*. [2002]). East of the Sierra de Comechingones, trenching of the Las Lagunas fault near the town of Sampacho (Figure 2A) revealed evidence of multiple possible earthquakes along the fault during Pleistocene time, with a moment magnitude of 6.6 estimated for one event occurring between 3700 and 2820 years BP [*Sagripanti and Villalba*, 2009]. Other historic events have been observed in the region of Sampacho, including two earthquakes in 1934 with depths of 20 km and maximum magnitudes near 6 (Figure 6a) [*Sagripanti et al*., 1998]. Although GPS studies spanning the Precordillera and the Sierras Pampeanas cannot discern E-W shortening within the Sierras de Córdoba [*Brooks et al*., 2003; *Kendrick et al*., 2006], the documentation of seismicity in this region indicates active deformation [*Alvarado et al*., 2005; *Mingorance*, 1991; *Richardson et al*., 2012].

3. Surface Fault Observations

[6] We collected structural and lithologic data from exposures along two of the east-dipping, range-bounding faults, the Sierra Chica and Sierra de Comechingones faults, as well as one west-dipping fault exposed near the town of Nono (Figures 2A and 3). These exposures provide the best opportunity to determine the style and timing of near-surface deformation in the Sierras de Córdoba. We then incorporate our data with previously published ages of footwall strata truncated by the faults. Previous studies have analyzed the exposures included in our study either individually or with

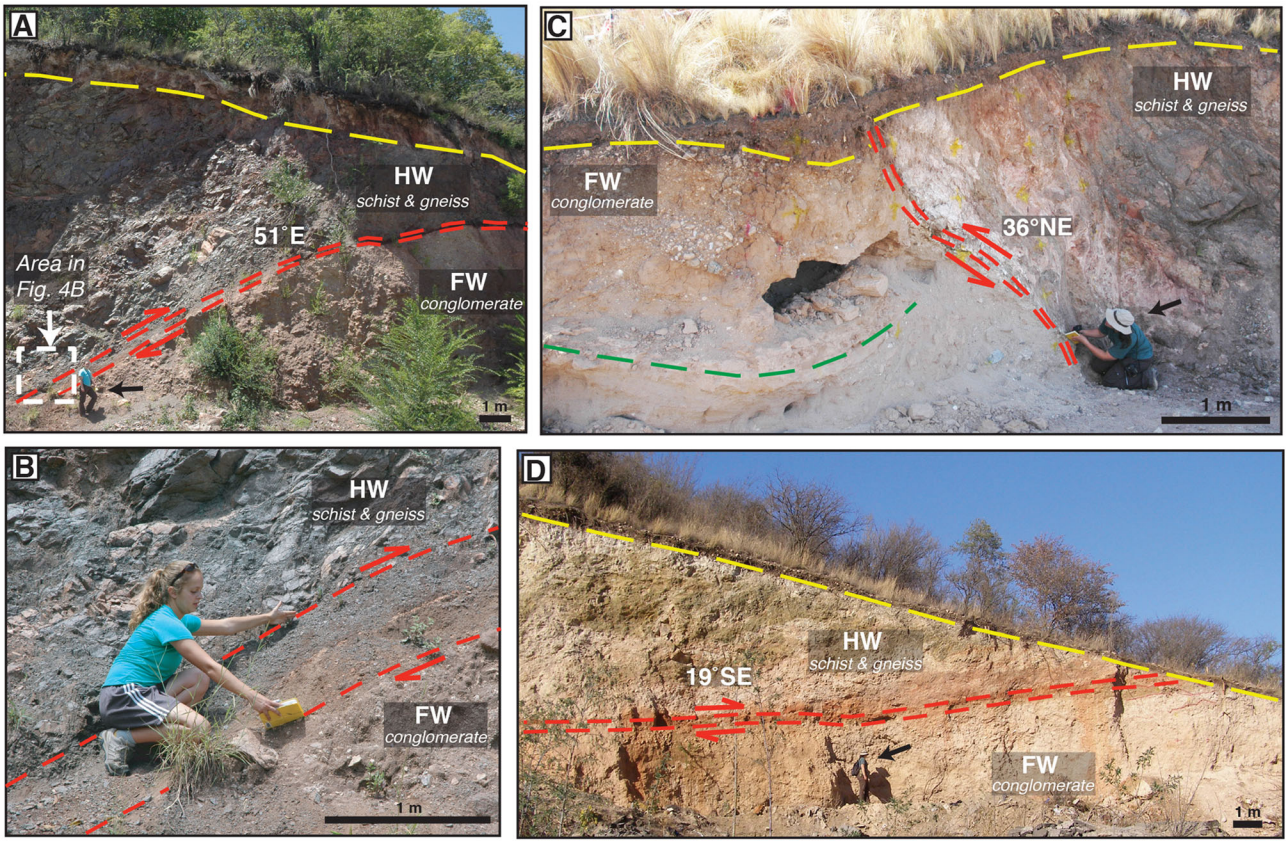

Figure 4. Exposures of the Sierra Chica fault with locations indicated in Figure 3A. Dashed red lines bound zones of fault gouge with arrows demonstrating the sense of motion, and dashed yellow lines indicate the depth of alteration from vegetation. (a and b) Exposure SC1 along a straight segment of the Sierra Chica fault near the town of Santa Rosa de Calamuchita, looking south. The fault zone has a trend of 000° at this site. A black arrow marks a person in Figure 4A for scale. (c) Exposure SC2 of the Potrero de Garay segment of the Sierra Chica fault near the Los Molinos reservoir, looking north. The fault trends 302° at this site. The dashed green line follows a fine sand layer illustrating the deformation of footwall strata due to activity along the fault. (d) Exposure at SC3 along the Sierra Chica fault near the town of Carlos Paz, looking south with a person (black arrow) for scale. The fault trends 061° at this site and is located along a segment of the fault that is concave to the west.

other local, smaller fault exposures [*Costa et al*., 2000, 2001, 2010]. Our goal, though, is to integrate data from major fault exposures throughout the Sierras de Córdoba to better constrain the age of near-surface fault displacement and to document the style of deformation at a regional scale. In the following section, we present a brief synthesis of key observations from the best fault exposures described by *Richardson* [2011].

3.1. Sierra Chica Fault

3.1.1. Observations

[7] The Sierra Chica fault, which forms the western boundary of the Sierra Chica range, trends roughly N-S and dips between 20° and 89°E along its curved trace (Figures 2A and 3A) [*Costa et al*., 2000; *Lencinas and Timonieri*, 1968; *Schmidt et al*., 1995; *Richardson*, 2011]. The southernmost exposure of the fault is located near the town of Santa Rosa de Calamuchita (SC1, Figure 3A). The fault at this exposure has an average trend of 000° and dips 51°E (Figure 4a) as defined by a 0.5–1 m zone of red fault gouge (Figure 4b). The hanging wall consists of highly fractured, late Proterozoic to Cambrian schist and gneiss. The footwall consists of an unorganized, cobble-boulder conglomerate with mainly gneiss and schist clasts (Figure 4B). Bedding measurements from an interbedded sandstone in the footwall yield an average apparent strike of 017° and dip of 18°E. Although there are no precise age constraints, a USGS database [*Costa et al*., 2000] reports the footwall strata as Quaternary in age and the fault at this site as being active during the past 15 ka, based on 13.5 m of displacement along the fault plane visible in the outcrop [*Costa et al*., 2001] and correlation to slip rates on Quaternary faults in similar tectonic regimes [*Costa et al*., 2000].

[8] North of Santa Rosa near the Los Molinos reservoir, the Sierra Chica fault (SC2, Figure 3A) has an average strike of 302° and dip of 36°NE with a 10–20 cm-thick zone of fault gouge (Figure 4C). The hanging wall consists of late Proterozoic to Cambrian schist, whereas footwall strata consist of well sorted, medium- and fine-grained sandstone with lenses of pebble-to-cobble conglomerate. The footwall strata are gently folded against the fault with a fold axis trending 015° and no discernible plunge (green dashed line,

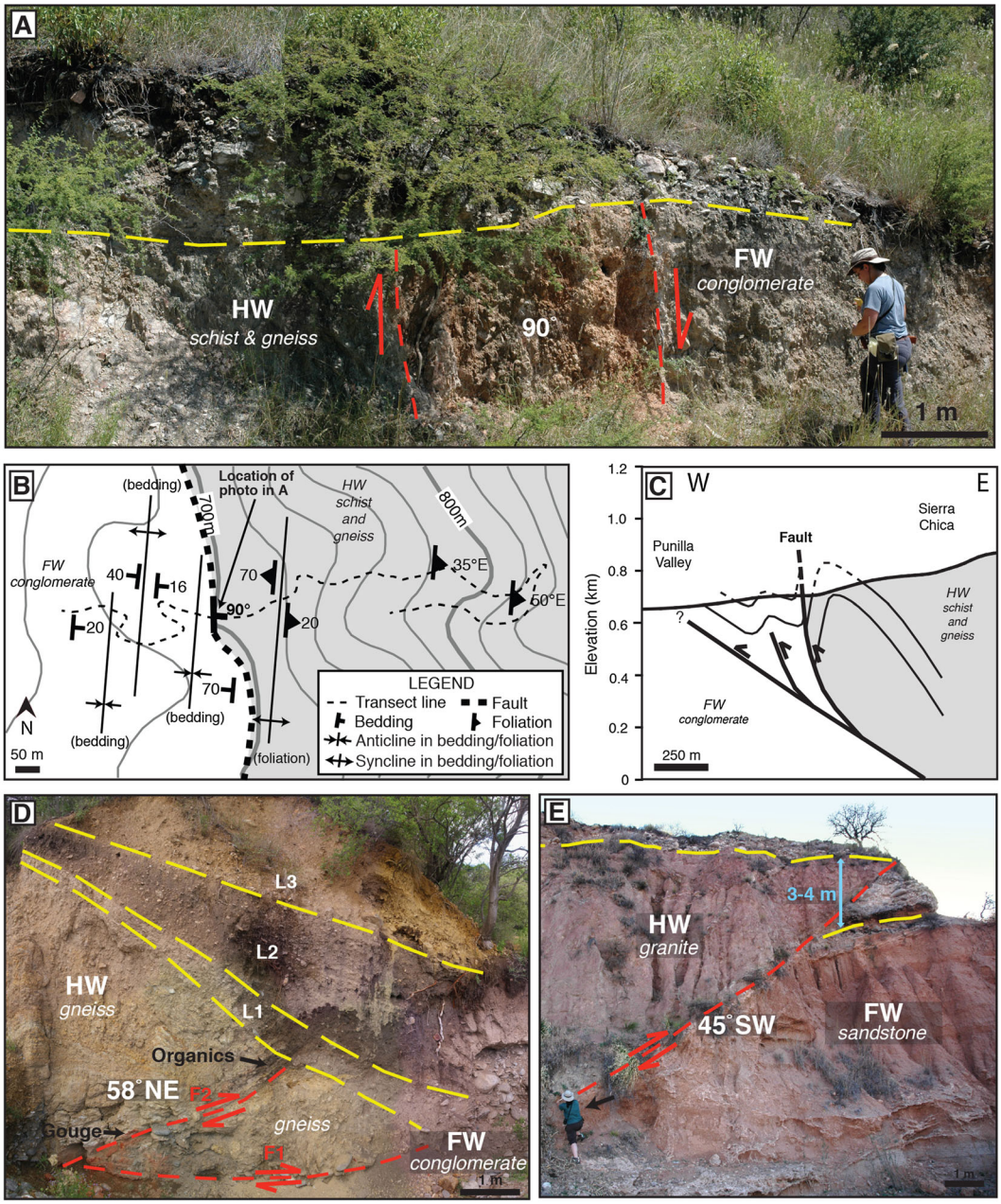

Figure 5. Fault exposures in the Sierras de Córdoba with locations indicated in Figures 3A and 3B. Dashed red lines bound the fault zones with arrows demonstrating the sense of motion, and dashed yellow lines indicate the depth of alteration from vegetation. (a) Exposure at SC4 along the Sierra Chica fault near the town of Bialet Masse, looking south. The fault trends 011° at this site, which is located along a straight segment of the Sierra Chica fault. The dashed yellow line indicates here the bottom of a young alluvial fan conglomerate covering both fault blocks. (b) Topographic contour map of 20 m intervals showing E-W transect across fault blocks at SC4. Nearly N-S trending lines show axes of anticlines and synclines in fault blocks with the dip of the limbs labeled. Individual foliation measurements are given in the hanging wall. (c) Schematic cross section at SC4 showing our interpretation of the fault in the subsurface and deformation in the fault blocks; looking north. (d) Exposure at SdC along the Sierra de Comechingones fault in the El Molino riverbed near the town of Merlo, looking south. Two fault splays are shown, the second of which (F2) bisects the gneiss in the hanging wall. The F2 fault splay trends 335°. The dashed yellow lines separate distinct layers that have formed above this fault exposure, which are likely alluvial fans or slumps that formed after the last activity along the fault. (e) Exposure along the Nono fault near the town of Nono, looking northwest. The fault zone trends at 101°. The dashed yellow line indicates the base of a Pleistocene alluvial fan conglomerate that overlies both fault blocks and is displaced 3–4 m by movement along the fault.

Figure 4C). The USGS database reports Holocene (<15 ka) movement along the fault at this outcrop [*Costa et al*., 2000].

[9] Moving northward to the town of Carlos Paz, there are two main exposures of the Sierra Chica fault (SC3, Figure 3A). At the more southern exposure, the fault on average strikes 061° with a dip of 19°SE (Figure 4D). Here the fault zone ranges between 30 and 100 cm in thickness and is characterized by red fault gouge. Small-scale asymmetric folds in the fault zone have a westward vergence. The late Proterozoic to Cambrian schist and gneiss of the hanging wall are juxtaposed over matrix-supported conglomerate with angular clasts of schist, gneiss, and quartz of the footwall. Bedding in the conglomerate, based on crude horizontal stratification, yields an average strike and dip of 128°, 21°SW. Quaternary motion along the fault has been documented in various seismic and tectonic studies of the adjacent valley, but the continuation of activity into the Holocene is unclear [*Costa et al*., 2000, and sources therein].

[10] The northernmost exposure of the Sierra Chica fault that we studied is located at Bialet Masse, 14 km north of Carlos Paz, where the fault trace shifts slightly to the east and assumes a more N-S trend (SC4, Figure 3A). At this site, the fault trends ~011°N with a near-vertical dip and separates late Proterozoic to Cambrian schist and gneiss of the hanging wall from boulder-cobble conglomerate of the footwall (Figure 5A). The 2 m-wide fault zone consists of fractured clasts within a red, coarse- to fine-grained matrix. A younger conglomerate (located above the dashed yellow line in Figure 5A) overlies both fault blocks and consists of angular, boulder clasts. The foliation of schist in the hanging wall block trends NW to NE and dips between 72°W near the fault and 35°–50°E about 500 m east of the fault (Figure 5B). This change in the orientation of foliation defines an asymmetric fold with vergence to the west (Figure 5C). In the footwall, bedding measurements taken within sandstone interbeds have N to NW trends with dips alternating between 20°E and 42°W with a dip of 70°W next to the fault zone (Figure 5B). The bedding measurements in the footwall strata delineate a series of folds in the conglomerate with fold axes trending ~015°N (Figure 5C). Movement along the fault appears to have occurred recently, even though no surface rupture was reported from the nearby M 6.5 16 January 1947 Villa Giardino earthquake [*Costa et al*., 2000].

3.1.2. Interpretation of the Sierra Chica Fault

[11] The Sierra Chica fault along the eastern margin of the Sierras de Córdoba has a strike and dip ranging between NW-NE and 19°–89°E based on our measurements. The hanging wall strata consist of late Proterozoic to Cambrian schist and gneiss that are part of the igneous-metamorphic basement rocks of the Sierras de Córdoba [e.g., *Martino*, 2003; *Martino et al*., 1995]. The locally deformed footwall strata are characterized by Pliocene to Pleistocene alluvial sequences [*Costa et al*., 2000, 2001]. Due to their clast composition and sedimentary structures, we interpret the footwall strata to be sourced predominantly from the adjacent hanging wall block (see *Richardson* [2011], for more details). Slickenline data at the fault exposure near Santa Rosa indicate a minor strike-slip component to the dominant dip-slip displacement suggestive of overall oblique reverse motion along the Sierra Chica fault [*Martino et al*., 1995; *Schmidt et al*., 1995].

3.2. Sierra de Comechingones Fault

3.2.1. Observations

[12] In the western part of the Eastern Sierras Pampeanas, the Sierra de Comechingones fault is well exposed along the El Molino Creek near the town of Merlo (SdC, Figure 3B). This exposure contains at least two imbricate faults (Figure 5D). The lower imbricate juxtaposes late Proterozoic to Cambrian gneiss in the hanging wall over clast-supported, cobble conglomerate in the footwall (F1, Figure 5D). The upper imbricate, defined by a zone of gouge, separates gneiss from gneiss, and tips out in a zone of organic-rich mudstone (F2; Figure 5D). Overlying both faults are three beds of matrix-supported conglomerate (L1, L2, and L3 on Figure 5D). The fault does not appear to continue upward into these strata.

3.2.2. Interpretation of the Sierra de Comechingones Fault

[13] At the studied exposure of the Sierra de Comechingones fault, the juxtaposition of late Proterozoic to Cambrian gneiss over Neogene and Quaternary conglomerate indicates a main component of reverse displacement. The poorly sorted strata overlying both fault imbricates were likely deposited after displacement and represent alluvial sequences or colluvium shed from the higher topography located directly east of the exposure.

[14] Dating of footwall strata from this fault exposure was conducted by *Costa and Vita-Finzi* [1996]. Two ^{14}C measurements from the organic-rich mudstone at the tip of the upper imbricate yield ages of 1080 ± 70 and 1310 ± 40 years BP, indicating at least 2 m of slip during the past 1300 years at this exposure [*Costa and Vita-Finzi*, 1996]. A more recent investigation defined the ages of fault-related deposits along this part of the fault system to range from 7.1 ± 0.4 ka to 350 ± 40 cal years BP [*Costa et al*., 2010]. From these results, the Sierra de Comechingones fault along the studied segment appears to have been active during Holocene time. This conclusion is consistent with historic seismicity recorded at the southern portion of the Sierra de Comechingones near the town of Sampacho (Figures 2A and 6A) [*Sagripanti et al*., 1998].

3.3. Nono Fault

3.3.1. Observations

[15] The Nono fault, exposed near the town of Nono, is the best example of a well-exposed, west-dipping fault in the study area (Figures 2s and 3b). The fault is defined by a 10–20 cmz-thick zone of red gouge that trends 101° and dips 45°SW (Figure 5E). The hanging wall consists of highly weathered granite and the footwall contains crudely laminated, coarse sandstone. A boulder conglomerate bed at the top of the exposure, overlying both the hanging wall and footwall, has been offset 3–4 m vertically (see yellow dashed line in Figure 5E).

3.3.2. Interpretation of the Nono Fault

[16] Due to its westward dip and shorter length (~30 km) relative to the east-dipping faults in the study area, we interpret the Nono fault to be a back thrust off of the east-dipping Pocho fault, which bounds the western margin of the Sierra de Pocho (Figure 3B). At the Nono fault exposure, the hanging wall granite is likely part of the Devonian Achala batholith (e.g., *Kraemer et al*., 1993). The sandstone in the

Table 1. Results of Apatite and Zircon (U-Th)/He Dating of the Achala Batholith in the Sierra Grande[a]

			(U-Th)/He Thermochronometry Results								
Sample	**Lat/Long**	**Elevat. (m)**	**4He (mol)**	**238U (mol)**	**235U (mol)**	**232Th (mol)**	**147Sm (mol)**	**Uncorr. Age (Ma)**	**Ft**	**Corr. Age (Ma)**	**Mean Age**
Apatite Ages											
	S31.61/ W064.83	2234									
TR 15			1.10E−12	3.11E−12	2.30E−14	1.78E−12	5.26E−12	235.64	0.781	300.1	
TR 15			9.78E−13	4.12E−12	3.05E−14	8.55E−13	8.63E−12	170.92	0.809	210.5	
TR 15			2.28E−12	6.36E−12	4.71E−14	8.53E−12	1.17E−11	207.12	0.788	261.7	**257 ± 45**
	S31.74/ W064.91	1623									
TR 9			4.55E−13	1.08E−12	7.96E−15	1.28E−12	2.11E−12	249.85	0.655	377.6	
TR 9			4.94E−13	2.02E−12	1.50E−14	3.81E−12	3.40E−12	129.92	0.703	184.1	
	S31.76/ W064.96	1076									
TR 3b			1.51E−13	9.32E−14	6.90E−16	3.65E−12	4.65E−12	121.96	0.850	143.4	
TR 3b			1.79E−14	3.56E−14	2.64E−16	2.81E−13	9.63E−13	130.96	0.772	169.3	
TR 3b			3.44E−14	6.12E−14	4.53E−16	3.34E−13	8.74E−13	185.05	0.807	228.8	**180 ± 44**
Zircon Ages											
	S31.74/ W064.91	1623									
TR 9			1.96E−11	6.47E−11	4.78E−13	1.81E−11		215.88	0.785	273.6	
TR 9			3.51E−12	1.54E−11	1.14E−13	2.49E−12		167.82	0.649	256.5	**265 ± 12**
	S31.74/ W064.94	1193									
TR 4			3.05E−12	1.50E−11	1.11E−13	7.18E−12		140.26	0.598	232.7	
TR 4			2.68E−12	1.62E−11	1.20E−13	2.67E−12		122.17	0.658	184.6	**209 ± 34**

[a]Blue circles and green diamonds in Figures 2B and 3B indicate the locations of the samples.

footwall is interpreted as a Pliocene to late Pleistocene fluvial-lacustrine deposit [*Kraemer et al*., 1993]. The offset conglomerate in the exposure represents a Pleistocene alluvial-fan deposit. The 3–4 m displacement of this conglomerate (Figure 5E) suggests that the Nono fault was active during Holocene time [*Kraemer et al*., 1993], and a slip rate of 0.2–1.0 mm/yr has been calculated for this fault [*Costa et al*., 2000].

3.4. Summary of Surface Fault Observations in the Sierras de Córdoba

[17] The major range-bounding faults of the Sierras de Córdoba dip between ~20° and 89°E at all surface fault exposures analyzed in our study. All these faults place late Proterozoic to Cambrian schist and gneiss over Neogene poorly dated alluvial strata. The style of deformation, the geometry of the faults, and the age of fault-truncated footwall strata suggest west-directed tectonic transport within the Sierras de Córdoba since at least Pliocene time. The Nono fault is the best-exposed example of smaller, west-dipping back thrusts within the ranges (Figure 3B).

[18] The age of Neogene and Quaternary basinal synorogenic strata adjacent to major ranges in the Sierras de Córdoba also provides some limited insight on the relative timing of deformation [e.g., *Massabie et al*., 2003]. In general, the age of basinal strata in the Punilla Valley related to activity along the Sierra Chica fault (Figure 3A) is mainly Miocene and Pliocene based on limited paleontological data [*Linares et al*., 1960; *Lencinas and Timonieri*, 1968]. These strata have a maximum thickness of 150 m based on well bore data. In the western part of the Sierras de Córdoba, the age and the thickness of basinal strata are poorly constrained. Due west of the Comechingones fault, in the Conlara Valley (Figure 3B), the thickness of the basinal strata has been estimated as very thin (less than 100 m thick where present) from magnetotelluric studies [*Chernicoff and Ramos*, 2003]. To the north, the Neogene strata in the Traslasierra Valley (Figure 3B) are best exposed at the Nono fault exposure, where there are ~12 m of Pliocene and ~4 m of Pleistocene strata exposed [*Kraemer et al*., 1993]. Farther west, the range-bounding Pocho fault is mostly covered by vegetation and modern alluvial fan and aeolian sediment [*Carignano*, 1999], but local exposures of footwall strata contain folded Carboniferous strata overlain by Quaternary strata [*Geuna and Escosteguy*, 2004]. The thickness of the Quaternary strata in the basin west of the Sierra de Pocho has not been well constrained. In general, however, there is a lack of thick sections of Neogene and Quaternary basinal strata in the western part of the Sierras de Córdoba based on our observations, previous geologic mapping, and limited well bore data [e.g., *França et al*., 1995]. Additional detailed geochronologic work on the synorogenic strata adjacent to each range will need to be done in future studies.

[19] We tentatively interpret the older Neogene basinal strata adjacent to the Sierra Chica fault relative to the younger strata adjacent to the Pocho fault to indicate that Neogene deformation in the Sierras de Córdoba may have begun in the east with the Sierra Chica range. Deformation has since propagated farther to the west and south with uplift of the Sierra de Comechingones and Sierra de Pocho. Consistent with this hypothesis is that the more active structures today appear to be those faults in the western part of the Sierras de Córdoba as documented in previously published paleoseismological and seismological studies [*Costa and*

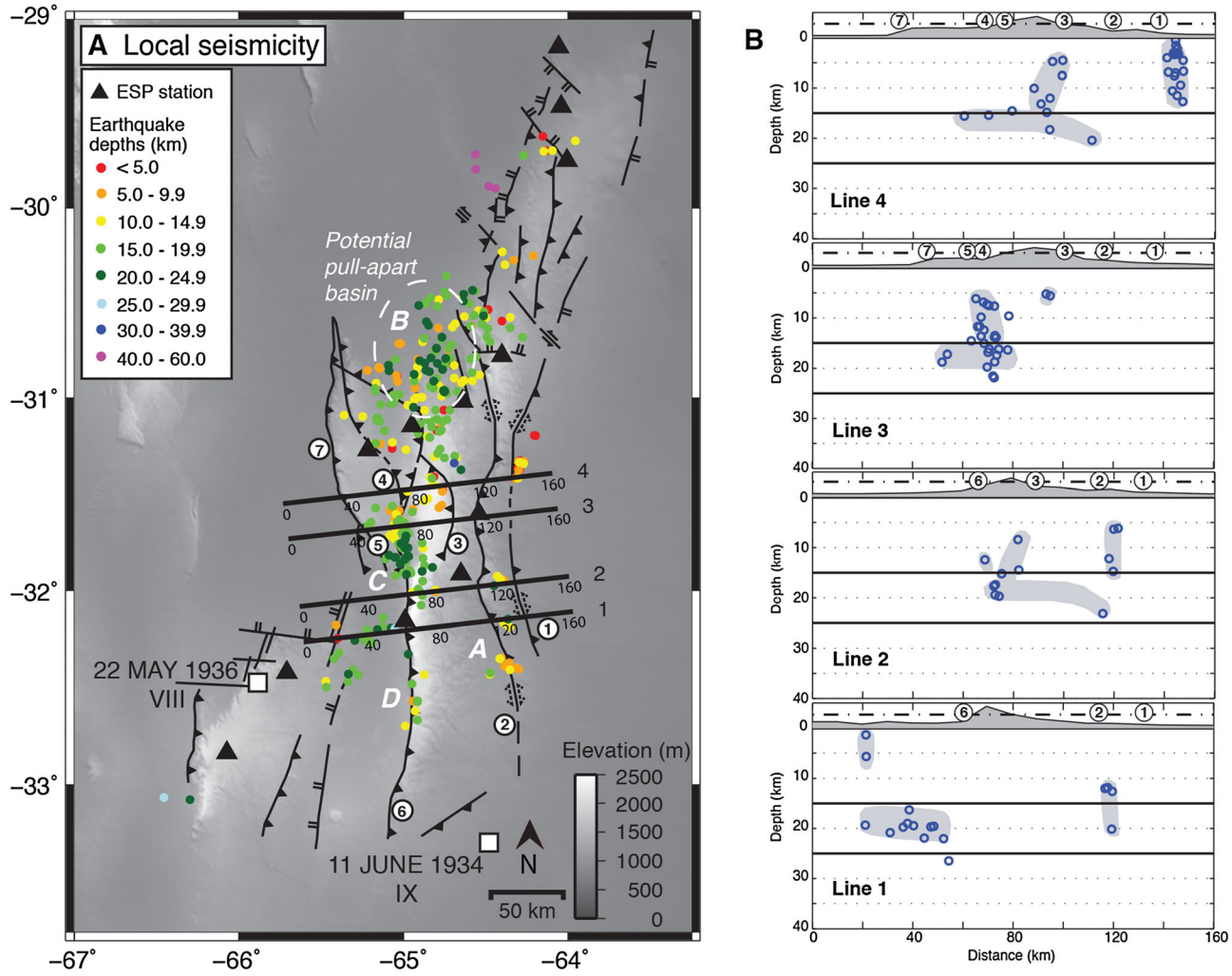

Figure 6. (a) Local shaded relief map with the double-difference hypocenters colored according to specified depth ranges, located using a velocity model with a fast lower crust [from *Richardson et al*., 2012]. The shallowest events locate along the eastern margin of the region and increase in depth to the west. Black triangles indicate the position of stations in the Eastern Sierras Pampeanas seismic array. Straight black lines indicate the position of seismicity cross sections in Figure 6B. Clusters of seismicity are labeled A, B, C, and D and are discussed in the text. A white dashed line indicates the location of a possible local pull-apart basin, and white squares mark the location of two historical events. (b) Cross sections through the Sierras de Córdoba plotting seismicity within 10 km of transect lines 1–4 presented in Figure 6A). Solid black lines at 15 km and 25 km depth indicate the approximate extent of the detachment and brittle-ductile transition zones. Planes of seismicity are highlighted with gray shading. Circled numbers correspond to the surface expression of major faults and are labeled according to Figure 2A.

Vita-Finzi, 1996; *Costa et al*., 2000, 2001, 2010; *Richardson et al*., 2012]. The timing of deformation that we propose for the Eastern Sierras Pampeanas fits well with the broad interpretation of regional Neogene uplift for this part of the Andean orogenic system [*Jordan and Allmendinger*, 1986; *Kay and Gordillo*, 1994; *Ramos et al*., 2002].

4. (U-Th)/He Thermochronometry

4.1. Methods

[20] To better understand the timing and amount of rock exhumation represented by the observed surface uplift for the central Sierras de Córdoba, we employed apatite and zircon (U-Th)/He thermochronometry to samples collected along a single range. This method is useful for determining the amount, timing, and rate of cooling as rocks are exhumed within the crust [*Ehlers and Farley*, 2003]. Rock exhumation is a result of both surface uplift and erosion, and in regions with little to no erosion, the rock uplift correlates to the surface uplift. In the (U-Th)/He system, the closure temperature for apatite ranges from 55° to 65°C and for zircon from 170° to 190°C, depending on cooling rate, grain size, and radiation damage [e.g., *Reiners et al*., 2004; *Schuster et al*., 2006; *Warnock et al*., 1997]. Depending on the geothermal gradient of the region, the depth of the closure temperature is ~2–3 km for apatite and 6–9 km for zircon [*Ehlers and*

Farley, 2003; *Rahl et al*., 2003]. If both apatites and zircons are dated, a longer portion of the cooling history of a rock is measured [*Ehlers and Farley*, 2003].

[21] For our study, we collected samples along the hanging wall of the Sierra Grande fault (Figure 2A), where some of the highest topography, and possibly exhumation, can be seen in the Sierras de Córdoba. The Sierra Grande consists mainly of the Devonian Achala batholith (Figure 2B), a medium- to coarse-grained granitic intrusion that is bounded to the west by the east-dipping Sierra Grande fault (Figure 2A) [*Demange et al*., 1996]. We sampled the bottom, middle, and top of the hanging wall as we moved east away from the range-bounding fault and up the slope of the Sierra Grande, yielding a total of 1200 m of elevation difference; sample details are outlined in Table 1. The analytical error of isotope measurements using mass spectrometry is small (1–2%) in comparison to the analytical reproducibility of a sample age. For that reason, the error we report for each mean age of a sample is the standard deviation of the sample aliquots (Table 1). For additional information on the methodology employed in this part of the study, see Appendix 1.

4.2. Results and Interpretation

[22] From the Sierra Grande, the mean apatite and zircon (U-Th)/He cooling ages range from 257±45 Ma to 180±44 Ma and 265±12 Ma to 209±34 Ma, respectively (Table 1). For sample TR 9 at midelevation (~1.6 km), the spread in the apatite ages between the two aliquots is large; therefore, we did not calculate a mean age for this sample (Table 1). The percent error of the data ranges from 4 to 20%, and the broad spread of the data is likely related to the old cooling ages of the grains, which is commonly observed in the (U-Th)/He dating method [see *Kirby et al*., 2002; *Warnock et al*., 1997]. Even though this preliminary data set is small, the results follow the expected trends in the age-elevation relationship. That is: (1) cooling ages increase with increasing elevations, and (2) the zircon cooling ages are older than the apatite cooling ages at the same elevation.

[23] The Permian to Early Jurassic ages indicate that during this time period, the Achala batholith was exhumed and cooled to the low temperatures of the upper 3 km of the crust. Although extension did not begin in this region until Early Cretaceous time [*Uliana et al*., 1989], the Eastern Sierras Pampeanas experienced a series of glaciations [*Gulbranson et al*., 2010], the San Rafael orogenic phase [*Ramos*, 2009], and a possible period of flat-slab subduction [*Ramos*, 2009] from late Carboniferous to late Permian time. The cooling ages of our analysis potentially relate to these tectonic events, but determining the processes responsible for these ages is beyond the scope of this paper and would require much more data.

[24] More important for our analysis is that from the preservation of these older ages, we can infer that the central Sierras de Córdoba have experienced limited exhumation (cooling) and burial (heating) since Early Jurassic time. Assuming a geothermal gradient of 25 ± 5°C/km, a surface temperature of 10°C, and an apatite U-Th/He closure temperature of 55–65°C, our data suggest exhumation and burial of no more than 1.5–3 km. A geothermal gradient of only 15–18°C/km has been suggested for the Late Miocene Andean foreland based on clay mineralogy studies in the Vinchina Basin [*Collo et al*., 2011] and a review of published thermochronometry ages from the Andean foreland [*Dávila and Carter*, 2013]. Assuming such a low geothermal gradient for the Sierras de Cordoba allows a maximum exhumation and burial of 3.7 km. However, it is important to point out that these studies are located >300 km west and north of our study area. As discussed earlier, our observations at fault exposures indicate displacement since at least Pliocene time, but the thermochronologic data suggest that this uplift did not cause any significant rock exhumation during the last ~5 Ma of Andean deformation. This interpretation is consistent with results from apatite fission track, K-Ar, and $^{40}Ar/^{39}Ar$ ages from the Sierra Grande near 31°S [*Jordan et al*., 1989]. From the relief of the Sierra Grande over the adjacent Traslasierra Valley, at least 1 km of the range has been exhumed due to surface uplift. The preservation of Jurassic planation surfaces [*Beltramone*, 2007; *Carignano et al*., 1999] and thin Neogene strata in the adjacent basins suggest that this landscape is youthful and has not experienced significant erosion. The limited amount of exhumation appears consistent with the fault exposure data that suggest mainly Pliocene and younger deformation in the Sierras de Córdoba.

5. Seismic Observations

[25] The Eastern Sierras Pampeanas has been interpreted as an area of active deformation in response to flat-slab subduction [*Jordan and Allmendinger*, 1986; *Costa and Vita-Finzi*, 1996; *Ramos et al*., 2002]. To quantify the location and style of deformation in the region, we analyzed data recorded by the temporary Eastern Sierras Pampeanas seismic array, which was composed of 12 stations oriented in north-south and northeast-southwest transects across the ranges (Figure 6A).

5.1. Local Seismicity in the Eastern Sierras Pampeanas

[26] From data collected between August 2008 and August 2009, we calculated single- and multiple-event locations for more than 400 local earthquakes detected by the network, most with estimated magnitudes of 2.5 or less [*Richardson et al*., 2012]. The locations of these events were determined using the same velocity model as that used to migrate receiver function arrival times to depths, as described below. Focal mechanisms calculated for some of the larger events recorded in the Sierras de Córdoba exhibit a heterogeneous distribution and style of deformation, displaying tensional, compressional, and strike-slip motion with no clear spatial pattern [*Richardson et al*., 2012]. However, solutions for many events include an oblique component, suggesting some amount of strike-slip motion in the deformation of the region. An earlier study that calculated moment tensors for crustal seismicity across the Sierras Pampeanas also identified an oblique component to deformation based on several right-lateral moment tensors [*Alvarado et al*., 2005]. *Richardson et al*. [2012] presented a more detailed analysis of the processing and uncertainties of the earthquake locations and focal mechanisms determined using the Eastern Sierras Pampeanas array. Only the main conclusions that relate to our tectonic interpretation of the Eastern Sierras Pampeanas are presented below.

[27] Figure 6 displays the regional distribution of crustal hypocenters and faults through the Eastern Sierras

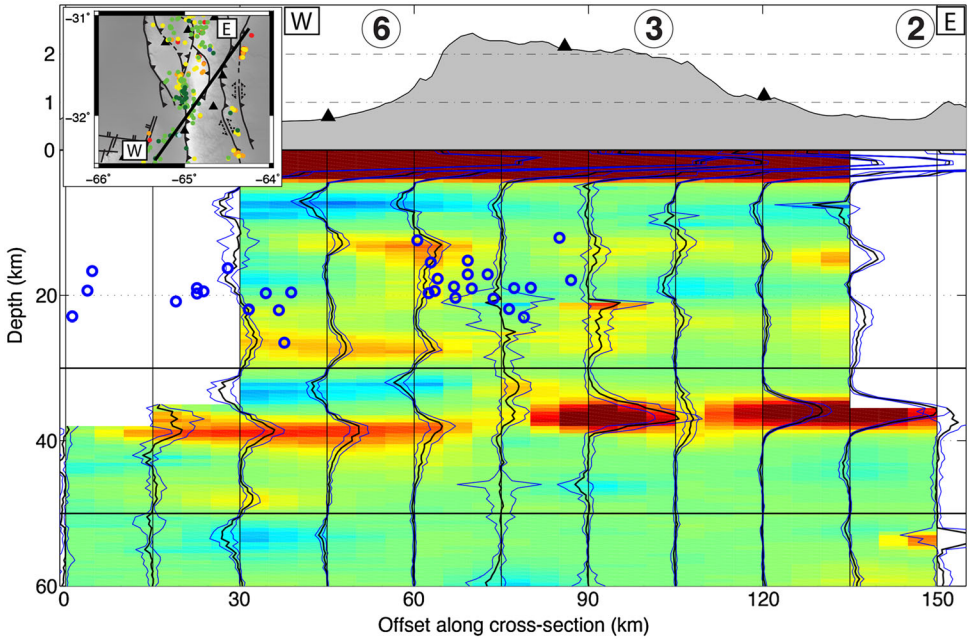

Figure 7. Receiver function cross section oriented NE-SW through the central portion of the study area, as indicated by the inset map. The transect orientation was chosen based on its proximity to the stations and lies near the southern transect presented by *Perarnau et al*. [2012]. Red colors mark positive receiver function arrivals corresponding to the depths where seismic velocities decrease for an upcoming wave traveling from deeper to shallower depths towards the seismic stations on the surface. Conversely blue colors mark the depths where seismic velocities increase as waves travel to shallower depths. Stacked amplitudes for each column of stacking bins are shown as heavy black lines with uncertainties based on bootstrap resampling indicated by thin blue lines. The high-amplitude positive phases at ~37 km depth mark the position of the Moho, and a lower amplitude phase in the midcrust at ~25 km depth likely indicates the base of the brittle-ductile transition. Seismicity within 10 km of the transect is overlaid on the receiver functions as blue circles. The locations of seismic stations (triangles) and fault traces (circled numbers) are indicated along the top of the cross section.

Pampeanas. Along the eastern margin of the Sierras de Córdoba, seismicity forms small clusters of events in the upper 15 km of the crust which trend near the surface trace of the Pampean Elevation and Sierra Chica faults (Figure 6A). In cross section lines 1, 2, and 4 (Figure 6B), these clusters appear to be linear and vertically oriented. We attribute the events to a continuous vertical structure trending northeast-southwest along the eastern margin of the area, which could be related to deformation along a reactivated suture between the Córdoba terrane and the Rio de la Plata craton (Figure 2B). An oblique component of motion from focal mechanisms across the region supports the possibility of strike-slip deformation along this vertical suture [*Richardson et al*., 2012]. From the data presented here, it is not clear how the vertical seismicity connects to the Sierra Chica fault nearby, because the vertical cluster in the north (line 4, Figure 6B) is east of the fault trace and the clusters in the south where epicenters are close to the trace of the fault are greater than 5 km deep (cluster A, Figure 6A; lines 1 and 2, Figure 6B).

[28] To the west of the Sierra Chica, seismicity deepens to between 5 km and 25 km depth with the majority of events located in two large clusters, labeled "B" and "C" in Figure 6A. In cluster B to the north, earthquakes are nearly evenly distributed between depths of 0 and 25 km and scattered underneath a broad topographic basin between the northern portion of the Sierra Chica fault and the Sierra de Pocho fault (see dashed circle in Figure 6A). Such a broad pattern of seismicity can result from crustal deformation across a large number of small faults that characterize an early stage of extensional faulting prior to the faults coalescing onto a single structure. In this interpretation, a pull-apart structure and the seismicity in cluster B would result from right-lateral oblique motion distributed across the Sierras de Córdoba (Figure 6A). An alternative interpretation of the formation of this basin is presented in *Dávila et al*. [2005] which interpret the ~1 km of basinal sediment identified in a local seismic survey to be dominantly of Miocene age. *Dávila et al*. [2005] proposed that this basin is part of a longer-wavelength (>500 km) pattern of subsidence driven by processes such as asthenospheric corner flow or lower crustal eclogitization. Smaller-scale density variations would then be needed to produce shorter-wavelength subsidence with scales less than ~300 km. Currently available observations cannot identify the timing of basin formation, but improved age constraints would help determine if the basin formed earlier or as a result of an ongoing process.

[29] Farther to the south, seismicity becomes more tightly clustered (cluster C, Figure 6A) near the junction of the Sierra Grande, Sierra de Pocho, and Sierra de Comechingones faults. The convergence of these faults appears to focus deformation into a localized region between 5 km and 25 km depth (line 3,

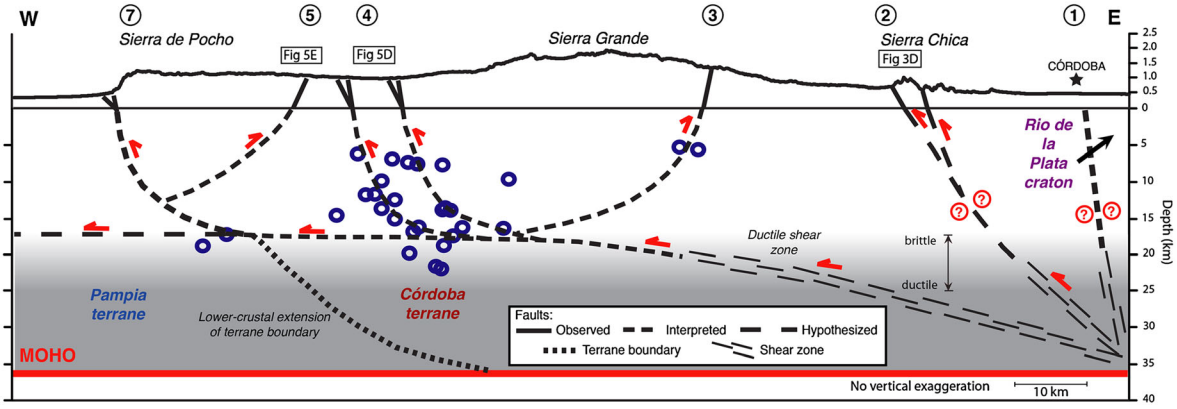

Figure 8. Structural cross section oriented E-W through the central Sierras de Córdoba (location follows seismicity cross-section line 3 presented in Figure 6), integrating results from the geologic and geophysical analyses described previously. A solid red line indicates the approximate depth of the Moho. Gray shading illustrates the ductily deforming lower crust beneath the Eastern Sierras Pampeanas, with the transition to brittle deformation indicated by the fade from gray to white. Blue circles indicate the epicenters of earthquakes located within 10 km of the transect. A dashed line at ~20 km depth indicates the position of the detachment beneath the Sierras de Córdoba as it extends from the east to the west, possibly becoming a ductile shear zone in the lower crust near the craton. Other dashed lines also correlate to the interpreted extent of faults, shear zones, or terrane boundaries. Reverse faults splay off this detachment zone to the surface, with arrows signifying motion along the faults. A shear zone with uncertain direction of motion (see question marks) is present in the east, with the Sierra Chica fault hypothesized as continuing to the detachment zone. Circled question marks note uncertainty in the sense of movement (either right lateral or left lateral) across the shear zone. Figure numbers correspond to outcrops that are related to the surface expression of faults in the subsurface while circled numbers correlate to fault names given in Figure 2A. The main ranges are labeled, and topography has no vertical exaggeration.

Figure 6B). Although the Sierra Grande fault appears active with seismicity between 5 and 15 km depth near horizontal offsets of 70 km along line 3 (Figure 6B), this and other range-bounding faults exhibit little activity along the majority of their lengths, including both the Sierra de Pocho and Sierra de Comechingones faults. Events in cluster D (Figure 6A), located directly below the trace of the east-dipping Sierra de Comechingones fault, occur mainly between 10 km and 20 km depth and are not attributed to the range-bounding fault. However, considering that fault scarp analyses in this area suggest that the recurrence interval for large events along the main thrust faults is 900–1200 years [*Sagripanti and Villalba*, 2009], we do not expect that a temporary deployment like the Eastern Sierras Pampeanas array would record a large compressional event along one of the large range-bounding faults. Instead, the array is more likely capturing the smaller-magnitude background seismicity of the region that is present between larger events. East of the Sierra Grande, the smaller west-dipping Schlaginweit fault (Figure 2A) appears active with seismicity along much of its curved trace (lines 2, 3, 4; Figures 6A and 6B), but it is unclear whether or not this fault connects to the Sierra Grande fault and the seismicity in cluster B.

[30] Beneath the central Sierras de Córdoba, seismicity generally aligns along a horizontal zone between 15 and 25 km depth (Figure 6B) and likely represents a midcrustal detachment zone near the transition from brittle to ductile deformation [*Richardson et al.*, 2012]. Similar horizontal detachments have been proposed beneath ranges in the northern and western parts of the Sierras Pampeanas [*Alvarado and Ramos*, 2011; *Cristallini et al.*, 2004; *González Bonorino*, 1950] and beneath the Laramide basement arches of the western North America [*Erslev*, 1986, 2005]. This detachment appears to be more or less continuous north-south beneath the ranges and to extend westward beneath the northern portion of the Sierras de San Luis (Line 1, Figure 6B). As discussed later in the text, based on the depth and distribution of seismicity, we propose that this detachment surface connects to the main faults in ranges farther to the west in the Sierras Pampeanas [*Gans et al.*, 2011].

5.2. Receiver Function Analysis

5.2.1. Methods

[31] To better resolve deeper crustal structures in the Eastern Sierras Pampeanas, we constructed a receiver function cross section through the central portion of the Sierras de Córdoba. Receiver functions are sensitive to discontinuities in seismic wave velocities and can be used to identify structures in the crust and upper mantle [e.g., *Phinney*, 1964; *Langston*, 1979]. From data recorded by the Eastern Sierras Pampeanas array, we used the *P* and *PP* phases of teleseismic events to calculate receiver functions that present converted *P*-to-*S* waves and stack them into a cross section sampling the central portion of the ranges.

[32] We stacked data from all azimuths that sample the same subsurface area to improve the signal-to-noise ratio and enhance laterally coherent crustal features. The spacing of the stacking bins used to generate the cross section is 15 km which averaged 40 receiver functions per bin and shared data between adjacent bins. To convert the arrival

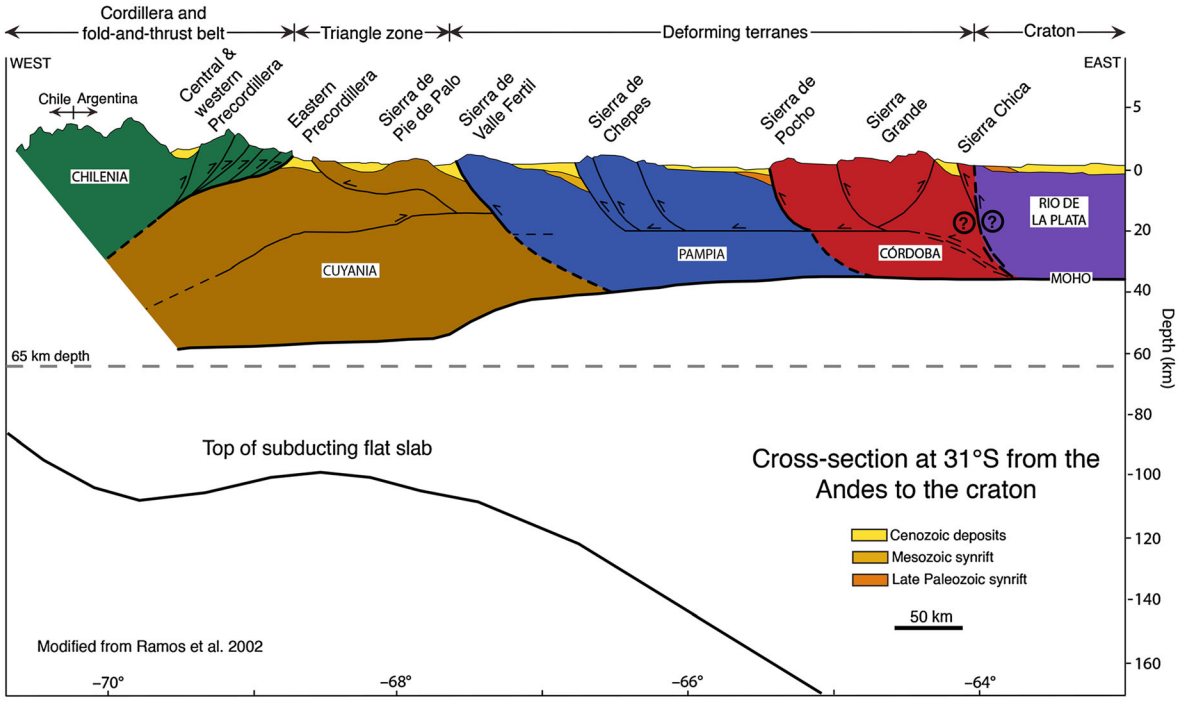

Figure 9. Regional geologic cross section spanning the Principal Cordillera in the Andes east to the stable Rio de la Plata craton [modified from *Ramos et al*., 2002]. A curved black line indicates the position of the flat slab beneath the South American plate [*Anderson et al*., 2007] and is extended eastward from *Alvarado et al*. [2009]. The upward bend of the subducting slab reflects the distribution of seismicity [*Anderson et al*., 2007] and receiver function arrivals [*Gans et al*., 2011] used to identify the position of the slab. Dashed gray line at 65 km depth is a reference for crustal thickness. The position of the Moho is adjusted according to *Gilbert et al*. [2006]. Thick black lines in the crust indicate the position of boundaries between terranes, which are modified from and labeled according to *Ramos* [2009]. Reverse faults in the deforming terranes sole into midcrustal detachments (horizontal line in deforming terranes). The structure of the Sierras de Córdoba has been modified according to results from this study. Basinal sediments at the surface are based on *Ramos et al*. [2002]. The Andean margin is divided into distinctly deforming regions, which are labeled accordingly at the top of the figure.

times of receiver function phases to depths, we used a local velocity model calculated for the region in which upper crustal velocities of 5.59 km/s extend to a depth of 5 km and are underlain by a higher velocity crust with velocities of 6.33 km/s [*Richardson et al*., 2012]. Last, we compare features in the receiver function stacks (Figure 7) to the locations of earthquakes detected by the seismic array in the Eastern Sierras Pampeanas.

[33] The location of the receiver function cross section presented here (Figure 7) lies close to the section presented by *Perarnau et al*. [2012] which was constructed from signals generated by deep local and regional events. Although high-frequency data (near 2 Hz) from deep local events better image the details of midcrustal structures, *Perarnau et al*. [2012] found that the lower-frequency teleseismic data (centered near 1 Hz) provide sampling over a broader azimuthal range. The teleseismic data are therefore better suited to illuminate the east-west extent of crustal structures. The thickness and general structure of the crust in the central portion of the Sierra de Córdoba appear similarly when comparing cross sections constructed from either local or teleseismic data, which provides confidence that features imaged in Figure 7 are robust.

5.2.2. Observations and Interpretations

[34] Along the cross section, sampling the central portion of the Sierras de Córdoba (Figure 7), a continuous high-amplitude converted phase at ~37 km depth indicates the position of the Moho where seismic speeds abruptly decrease from the upper mantle to the lower crust. Above the Moho under the western margin of the study area, there appears to be an intracrustal structure based on a midcrustal arrival. The strongest and most continuous midcrustal arrival lies at depths between 25 and 27 km and extends westward from the area of high elevations of the Sierra Grande at horizontal offsets of 30–60 km along the cross-section line (Figure 7). The receiver function stacks produced by *Perarnau et al*. [2012] also possess an arrival in this depth range. Seismicity near this midcrustal arrival tends to locate in a horizontal zone between 18 and 23 km depth. Beneath Sierra Grande, at horizontal offsets between 60 and 90 km along the cross section, additional midcrustal arrivals exist at depths of ~13 and 20 km. Similarly, the distribution of seismicity also broadens to shallower depths beneath the Sierra Grande.

[35] Because the midcrustal arrival near 25 km depth separates seismic and aseismic portions of the crust, we interpret this feature to reflect the transition from brittle upper crust to

ductile lower crust. The brittly deformed upper crust would then slow the upgoing waves, causing a velocity transition at this boundary and therefore a converted phase in the receiver function. The proximity of the converted phase with the horizontal zone of seismicity suggests that the midcrustal detachment zone beneath the Sierra Grande is located near or within the brittle-ductile transition zone. Range-bounding faults within the Eastern Sierras Pampeanas likely sole into this horizontal detachment zone near 20 km depth. Similar interpretations have been proposed for range-bounding faults in the Western Sierras Pampeanas using the relationship between hanging wall and fault geometries measured at the surface [*González Bonorino*, 1950; *Jordan and Allmendinger*, 1986; *Ramos et al*., 2002]. The detachment and brittle-ductile transition both appear to continue westward from the southern portion of the Sierras de Córdoba into the adjacent terrane (see Figures 6B and 7) and are not visible beneath the ranges to the east. The shallower, more localized arrivals in the upper crust may result from slower velocities related to deformed rock near range-bounding faults, especially in locations where earthquakes are present. Otherwise, they could reflect compositional changes between granitic intrusions and metamorphic rock.

6. Discussion

6.1. Integration of Data and the Structural Configuration of the Eastern Sierras Pampeanas

[36] By integrating multiple data sets collected at a range of scales, including surface fault and stratigraphic observations, exhumation data, local crustal seismicity, and receiver functions, we have constructed an E-W cross section that shows our interpretation of the tectonic configuration of the Eastern Sierras Pampeanas (Figure 8). The surface observations of fault exposures and stratigraphic thicknesses suggest that the uplift and deformation of the ranges have occurred since at least Pliocene time and continue to the present; this deformation may have progressed from east to west. From our preliminary thermochronometry study, we suggest that the Sierra Grande in the center of the region has been exhumed less than 3 km; this finding is consistent with fairly young deformation. At a larger scale, our subsurface observations of local seismicity illustrate several active structures in the Eastern Sierras Pampeanas including both east-dipping and west-dipping reverse faults that sole into a horizontal detachment zone between 15 and 20 km depth (Figure 6A-B). Finally, receiver function phases show the Moho at ~37 km depth and possibly a lower boundary where deformation transitions from the brittle to ductile regime at ~25 km depth (Figure 7).

[37] In the local cross section in Figure 8, a horizontal red line at 37 km depth represents the position of the Moho. At shallower depths, the midcrustal detachment beneath the Sierras de Córdoba is located between 15 and 20 km depth. This structure may increase in depth toward the terrane suture along the eastern margin of the ranges (Figure 8), which is suggested by the slight increase in depth of seismicity along the detachment between horizontal offsets of 90 to 120 km on Line 4 (Figure 6B). As the detachment zone continues eastward below the transition to ductile deformation, it may become a ductile shear zone that soles into the Moho near the boundary between the craton and terrane (Figure 8). Crustal shortening along this shear zone would then exhume deep crustal material in an aseismic manner, accounting for the lack of seismicity along the detachment at the eastern margin of the region (Figure 6B). The lack of a strong arrival in the receiver function cross section at these depths (Figure 7) may be related to crustal anisotropy that could cause phases from different azimuths to cancel out when they are averaged together. A detailed analysis of the crustal anisotropy beneath the Sierras de Córdoba is needed and is being addressed by ongoing studies. As the detachment flattens westward into a zone at 15–20 km depth beneath the Sierra Grande, the transport of crustal material over this ramp may explain the high topography of this range. In Figure 7, both the receiver function phases and located seismicity suggest that the detachment zone may continue west of the Sierras de Córdoba and extend into the adjacent terrane (Figure 8). During the development of these ranges, upper crustal material in the Córdoba terrane has been transported westward along the detachment (Figure 8). From the basin stratigraphy and age of footwall strata presented in this study, westward tectonic transport was most likely ongoing by at least Pliocene time.

[38] We attribute the vertical zone of seismicity along the eastern edge of the Sierras de Córdoba to deformation along a potentially continuous, vertical boundary between the Córdoba terrane and the Rio de la Plata craton (Figures 2 and 8) [*Richardson et al*., 2012]. This location of the suture between the blocks corresponds to a change in resistivity between the accreted terrane and the craton as shown in previously published magnetotelluric cross sections [*Booker et al*., 2004; *Favetto et al*., 2008]. The possible northeastward shift in location of the vertical zone of seismicity between cross sections (Figure 6A–B) could indicate a NNE-SSW trend for the boundary along the eastern margin of the Sierras de Córdoba (Figures 1 and 2). This apparent trend of the boundary also is depicted in terrane boundary interpretations by *Ramos et al*. [2004] and in magnetotelluric studies by *Chernicoff and Zappettini* [2004].

6.2. Regional Implications

[39] Our investigation has better delineated the easternmost region of active crustal deformation in central Argentina. These results impact our interpretation of regional deformation that may be related to shallow subduction at ~32°S along the western margin of South America (Figure 1). At this latitude in the west, the modern configuration of the Andes illustrates several of the processes associated with active flat-slab subduction (Figure 9) [e.g., *Jordan and Allmendinger*, 1986; *Kay and Abbruzzi*, 1996; *Ramos*, 2009; *Ramos et al*., 2002; *Kay and Mpodozis*, 2002]. From Miocene to modern time, shallowing of the subducting plate led to the propagation of magmatism and crustal deformation into the interior of the continent. At present, the flat slab at 100 km depth underlies the Andean Cordillera and Precordillera fold-and-thrust belt and the Western Sierras Pampeanas basement-involved uplifts within the westernmost belt of accreted terranes (Figures 1 and 9). In the Cuyania terrane to the east, a regional triangle zone accommodates the change from west-dipping to east-dipping structures [*Zapata and Allmendinger*, 1996]. Due to shortening and subduction erosion related to flat-slab processes, the greatest amounts of crustal thickening [*Fromm et al*., 2004; *Gilbert et al*., 2006] and lithospheric

thinning [*Kay and Abbruzzi*, 1996] in the overriding plate occur within the Cuyania terrane. From studies of *Pn* phase velocities, receiver functions, and geochemical signatures of magmas, the crustal thickness of the upper plate in this terrane extends close to 65 km depth [*Fromm et al*., 2004; *Alvarado et al*., 2005; *Gans et al*., 2011], and the lower crust may be partially eclogitized due to crustal thickening [*Gilbert et al*., 2006; *Kay and Mpodozis*, 2001; *Snyder et al*., 1990].

[40] East of the triangle zone are the ranges of the Sierras Pampeanas, within which the accreted terranes forming the crust shorten through the uplift of metamorphic and igneous rocks along reverse faults that, in general, bound the western margins of the ranges (Figure 9). Below this area, the subducting slab is located at greater than 120 km depth [*Alvarado et al*., 2009; *Anderson et al*., 2007] and crustal thicknesses between terranes vary from 35 to 40 km [*Alvarado et al*., 2007; *Gans et al*., 2011]. Modern deformation of the western portion of the Sierras Pampeanas is observed through ENE-directed shortening from the GPS velocity field in this region [*Brooks et al*., 2003]. Previous interpretations of the structural configuration of this region are based dominantly on surface observations and show range-bounding faults continuing to the Moho at depth [e.g., *Ramos et al*., 2002]. From our recent observations of the surface and subsurface of the eastern portion of the Sierras Pampeanas, we show that the range-bounding faults that are not terrane boundaries sole into midcrustal detachment zones near the brittle-ductile transition (Figure 9). A similar fault configuration has been proposed for ranges in the western parts of the Sierras Pampeanas based on surface observations of fault dip and the tilt of hanging wall blocks [*González Bonorino*, 1950; *Jordan and Allmendinger*, 1986]. A recent study of receiver functions spanning much of the Sierras Pampeanas to the west of our study area shows that midcrustal converted phases, corresponding to possible detachment zones, appear to vary in depth between terranes [*Gans et al*., 2011]. Despite these depth variations, results from our study in the east suggest that these detachments may cross boundaries between some terranes (Figures 6 and 7).

[41] Along the eastern margin of the Sierras Pampeanas, there appears to be an active near-vertical deformation zone along the boundary between the Rio de la Plata craton and the Córdoba terrane, which formed during Paleozoic time. The reactivation of the suture is a clear example of deformation throughout the Sierras Pampeanas being strongly influenced by the presence of preexisting crustal structures, as identified by *Ramos et al*. [2002] and *Alvarado and Ramos* [2011].

[42] In our modified model of crustal deformation from the Andean Cordillera to the craton at 32°S (Figure 9), increased coupling between the subducting flat slab and the overriding plate beneath the Cordillera [*Gutscher*, 2002; *Gutscher and Peacock*, 2003] results in the propagation of Neogene and Quaternary crustal deformation eastward to the Rio de la Plata craton. Below the craton, the subducting plate deepens to ~200 km [*Cahill and Isacks*, 1992; *Alvarado et al*., 2009; *Anderson et al*., 2007] and is therefore unlikely to be coupled to the lithosphere. Neogene and Quaternary deformation of the overlying region may have been facilitated by thermal weakening of the crust from the preceding eastward sweep of magmatism as the slab shallowed [*Kay and Mpodozis*, 2002]. Shortening across the Sierras Pampeanas is accommodated along east-dipping oblique reverse faults that sole into midcrustal detachment zones (Figure 9). As deformation reaches the eastern margin of the Córdoba terrane, the Rio de la Plata craton acts as a rigid backstop to crustal shortening and forces deformation to propagate back to the west into the belt of terranes. The ranges in the Eastern Sierras Pampeanas have experienced surface uplift but only little exhumation since deformation began in Neogene time and appear to be actively deforming in response to far-field flat-slab subduction.

7. Conclusions

[43] Results from our study refine the configuration and timing of active crustal deformation inboard of a region of active flat-slab subduction along the Andean margin. From surface observations, we interpret Neogene and Quaternary deformation within the region to have occurred on a series of east-dipping oblique-reverse faults beginning by at least Pliocene time and continuing to present. These faults juxtapose late Proterozoic to Cambrian metamorphic rocks over Neogene and Quaternary alluvial strata. Footwall stratigraphy suggests a progression of uplift from east to west within the Sierras de Córdoba, beginning with the Sierra Chica and Sierra Grande in Miocene/Pliocene time and progressing to the Sierra de Comechingones, Sierra de Pocho, and Sierra de Nono by late Pliocene to Pleistocene time.

[44] Integrating seismic observations of the subsurface with our geologic observations indicate that deformation in the Eastern Sierras Pampeanas occurs along oblique reverse faults that sole into a detachment zone between 15 and 20 km depth, which is near the brittle-ductile transition zone. The crust within the Sierras Pampeanas thins from west to east and is ~37 km thick beneath the Eastern Sierras Pampeanas. To the east of the Sierras Pampeanas, the Rio de la Plata craton acts as a rigid backstop to the eastward propagation of deformation driven by the subducting slab. Upper crustal deformation appears to propagate westward along the midcrustal detachment that extends across terrane boundaries into the Western Sierras Pampeanas.

Appendix A

[45] The apatite and zircon grains were separated using standard magnetic and heavy liquid separation techniques and were picked under a binocular microscope to avoid defects, inclusions, and impurities. Aliquots of multiple apatite grains (three to four grains) and single zircon grains were analyzed for ^{4}He in the noble gas laboratory at Lehigh University in Bethlehem, Pennsylvania, USA. Apatite and zircon grains were heated in a resistant furnace to 1100°C for 15 min and 1350°C for 60 min, respectively, and analyzed for ^{4}He by isotope dilution utilizing a ^{3}He spike and quadrupole mass spectrometry. After helium analysis, the samples were sent to the University of Arizona at Tucson, AZ, USA, for uranium, thorium, and samarium measurements using ICP-MS.

[46] **Acknowledgments.** We are grateful to IRIS and the PASSCAL Instrument Center (which are supported by NSF Cooperative Agreement EAR-0552316) for their help and support throughout the deployment of the Eastern Sierras Pampeanas seismic array. We appreciate the assistance and generosity of Jorge Sfragulla and Daniel Serra at the Córdoba office of the Servicio Geológico Minero Argentino (SEGEMAR). We are also thankful for the assistance provided by students from Purdue University, the universities of Córdoba and San Juan, and Colorado College during the installment, servicing, and demobilization of the seismic array. Insightful and careful reviews by Teresa Jordan and Suzanne Kay improved the manuscript. Grants from Exxon-Mobil helped support the exhumation history presented here. The National Science Foundation supported this research and the deployment of the ESP seismic array under grants EAR-0739001 and EAR-0738935.

References

Alvarado, P., and V. Ramos (2011), Earthquake deformation in the northwestern Sierras Pampeanas of Argentina based on seismic waveform modeling, *J. Geodyn.*, *51*, 205–218.

Alvarado, P., B. C. Machuca, and S. L. Beck (2005), Comparative seismic and petrographic crustal study between the Western and Eastern Sierras Pampeanas region, Argentina, *Rev. Asoc. Geol. Argent.*, *60*, 787–796.

Alvarado, P., S. Beck, and G. Zandt (2007), Crustal structure of the south-central Andes Cordillera and backarc region from regional waveform modelling, *Geophys. J. Int.*, *170*, 858–875, doi:10.1111/j.1365-246X.2007.03452.x.

Alvarado, P., M. Pardo, H. Gilbert, S. Miranda, M. Anderson, M. Saez, and S. Beck (2009), Flat-slab subduction and crustal models for the seismically active Sierras Pampeanas region of Argentina, *Mem. Geol. Soc. Am.*, *204*, 261–278.

Anderson, M. L., P. Alvarado, G. Zandt, and S. Beck (2007), Geometry and brittle deformation of the subducting Nazca Plate, Central Chile and Argentina, *Geophys. J. Int.*, *171*, 419–434.

Beltramone, C. A. (2007), Las superficies de erosión en las Sierras Pampeanas de Córdoba: Algunas consideraciones sobre su génesis, *Rev. Asoc. Geol. Argent.*, *62*, 478–82.

Booker, J. R., A. Favetto, and M. C. Pomposiello (2004), Low electrical resistivity associated with plunging of the Nazca flat slab beneath Argentina, *Nature*, *429*, 399–403.

Brooks, B. A., M. Bevis, R. Smalley Jr., E. Kendrick, R. Manceda, E. Lauria, R. Maturana, and M. Araujo (2003), Crustal motion in the Southern Andes (26°-36°S): Do the Andes behave like a microplate?, *Geochem. Geophys. Geosyst.*, *4*(10), 1085, doi:10.1029/2003GC000505.

Cahill, T. A., and B. L. Isacks (1992), Seismicity and shape of the subducted Nazca Plate, *J. Geophys. Res. 97*, 17,503–17,529.

Carignano, C. (1999), Late Pleistocene to recent climate change in Córdoba Province, Argentina: Geomorphological evidence, *Quat. Int.*, *57-58*, 117–134.

Carignano, C., M. Cioccale, and J. Rabassa (1999), Landscape Antiquity of the Central-Eastern Sierras Pampeanas (Argentina): Geomorphological Evolution since Gondwanic Times, *Z. Geomorphol. Neue Folge*, *118*, 245–268.

Chernicoff, C. J., and V. A. Ramos (2003), El basamento de la sierra de San Luis: Nuevas evidencias magnéticas y sus implicancias tectónicas, *Rev. Asoc. Geol. Argent.*, *58*, 511–24.

Chernicoff, C. J., and E. O. Zappettini (2004), Geophysical evidence for terrane boundaries in South-Central Argentina, *Gondwana Res.*, *7*, 1105–16.

Collo, G., F. M. Dávila, J. Nóbile, R. A. Astini, and G. Gehrels (2011), Clay mineralogy and thermal history of the Neogene Vinchina Basin, central Andes of Argentina: Analysis of factors controlling the heating conditions, *Tectonics*, *30*, TC4012, doi:10.1029/2010TC002841.

Costa, C. H., and C. Vita-Finzi (1996), Late Holocene faulting in the southeast Sierras Pampeanas of Argentina, *Geology*, *24*, 1127–1130.

Costa, C. H., M. N. Machette, R. L. Dart, H. E. Bastias, J. D. Paredes, L. P. Perucca, G. E. Tello, and K. M. Haller (2000), Map and database of Quaternary faults and folds in Argentina, *U.S. Geol. Surv. Open File Rep.*, 00-0108.

Costa, C. H., M. V. Murillo, G. L. Sagripanti, and C. E. Gardini (2001), Quaternary intraplate deformation in the southeastern Sierras Pampeanas, Argentina, *J. Seismol.*, *5*, 399–409.

Costa, C. H., W. Ricci, L. A. Owen, W. J. Johnson, A. Halperin, and E. A. Ahumada (2010), Holocene paleoearthquake clustering along a Sierras Pampeanas (Argentina) bounding fault?, Abstract T42A-05 presented at 2010 Fall Meeting, AGU, San Francisco, Calif., 13–17 Dec.

Cristallini, E. O., L. Giambiagi, and R. W. Allmendinger (2004), True three-dimensional trishear: A kinematic model for strike-slip and oblique deformation, *Geol. Soc. Am. Bull.*, *116*, 938–952.

Dávila, F. M., and A. Carter (2013), Exhumation history of the Andean broken foreland revisited, *Geology*, *41*, 443–446.

Dávila, F. M., R. A. Astini, and T. E. Jordan (2005), Cargas subcorticales en el antepaís andino y la planicie pampeana: evidencias estratigráficas, topográficas y geofísicas, *Rev. Asoc. Geol. Argent.*, *60*, 775–86.

Demange, M., J. O. Alverez, L. Lopez, and J. J. Zarco (1996), The Achala Batholith (Córdoba, Argentina): A composite intrusion made of five independent magmatic suites. Magmatic evolution and deuteric alteration, *J. South. Am. Earth Sci.*, *9*, 11–25.

Ehlers, T. A., and K. A. Farley (2003), Apatite (U-Th)/He thermochronometry: Methods and applications to problems in tectonic and surface processes, *Earth Planet. Sci. Lett.*, *206*, 1–14.

Erslev, E. A. (1986), Basement balancing of Rocky Mountain foreland uplifts, *Geology*, *14*, 259–262.

Erslev, E. A. (2005), 2D Laramide geometries and kinematics of the Rocky Mountain, Western U.S.A., in *The Rocky Mountain Region—An Evolving Lithosphere: Tectonics, Geochemistry, and Geophysics, Geophys. Monogr. Ser.*, vol., 154, edited by K. E. Kalstrom and G. R. Keller, pp. 7–20, AGU, Washington, D. C. doi:10.1029/154GM02.

Favetto, A., M. C. Pomposiello, M. Lopez de Luchi, and J. R. Booker (2008), 2D Magnetotelluric interpretation of the crust electrical resistivity across the Pampean terrane-Río de la Plata suture, in central Argentina, *Tectonophysics*, *459*, 54–65.

França, A. B., et al. (1995), Phanerozoic Correlation in Southern South America, in *Petroleum basins of South America, AAPG Memoir 62*, edited by. A. J. Tankard, R. Suárez, and H. J. Welsink, *AAPG Mem.*, *62*, 129–161.

Fromm, R., G. Zandt, and S. L. Beck (2004), Crustal thickness beneath the Andes and Sierras Pampeanas at 30°S inferred from Pn apparent phase velocities, *Geophys. Res. Lett.*, *31*, L06625, doi:10.1029/2003GL019231.

Gans, C. R., S. L. Beck, G. Zandt, H. Gilbert, P. Alvarado, M. Anderson, and L. Linkimer (2011), Continental and oceanic crustal structure of the Pampean flat slab region, western Argentina, using receiver function analysis: New high-resolution results, *Geophys. J. Int.*, *186*, 45–58, doi: 10.1111/j.1365-246X.2011.05023.x.

Geuna, S. E., and L. D. Escosteguy (2004), Palaeomagnetism of the Upper Carboniferous-Lower Permian transition from Paganzo basin, Argentina, *Geophys. J. Int.*, *157*, 1071–1089.

Gilbert, H., S. Beck, and G. Zandt (2006), Lithospheric and upper mantle structure of central Chile and Argentina, *Geophys. J. Int.*, *165*, 383–398.

González Bonorino, F. (1950), Algunos problemas geológicos de las Sierras Pampeanas, *Rev. Asoc. Geol. Argent.*, *5*, 81–110.

Gordillo, C. E., and A. Linares (1981), Geocronología y petrografía de las vulcanitas terciarias del Departamento de Pocho. Provincia de Córdoba, *Rev. Asoc. Geol. Argent.*, *36*, 380–388.

Gulbranson, E. L., I. P. Montañez, M. D. Schmitz, C. O. Limarino, J. L. Isbell, S. A. Marenssi, and J. L. Crowley (2010), High-precision U-Pb calibration of Carboniferous glaciation and climate history, Paganzo Group, NW Argentina, *Geol. Soc. Am. Bull.*, *122*, 1480–1498.

Gutscher, M. (2002), Andean subduction styles and their effect on thermal structure and interplate coupling, *J. South. Am. Earth Sci.*, *15*, 3–10.

Gutscher, M., and S. M. Peacock (2003), Thermal models of flat subduction and the rupture zone of great subduction earthquakes, *J. Geophys. Res.*, *108*(B1), 2009, doi:10.1029/2001JB000787.

Jordan, T. E., and R. W. Allmendinger (1986), The Sierras Pampeanas of Argentina: A modern analogue of Rocky Mountain foreland deformation, *Am. J. Sci.*, *286*, 737–764.

Jordan, T. E., B. L. Isacks, R. W. Allmendinger, J. A. Brewer, V. A. Ramos, and C. J. Ando (1983), Andean tectonics related to geometry of subducted Nazca plate, *Geol. Soc. Am. Bull.*, *94*, 341–361.

Jordan, T. E., P. Zeitler, V. A. Ramos, and A. J. W. Gleadow (1989), Thermochronometric data on the development of the basement peneplain in the Sierras Pampeanas, Argentina, *J. South. Am. Earth Sci.*, *2*, 207–222.

Kay, S. M., and J. M. Abbruzzi (1996), Magmatic evidence for Neogene lithospheric evolution of the central Andean "flat-slab" between 30°S and 32°S, *Tectonophysics*, *259*, 15–28.

Kay, S. M., and C. E. Gordillo (1994), Pocho volcanic rocks and the melting of depleted continental lithosphere above a shallowly dipping subduction zone in the central Andes, *Contrib. Mineral Petrol.*, *117*, 25–44.

Kay, S. M., and C. Mpodozis (2001), Central Andean ore deposits linked to evolving shallow subduction systems and thickening crust, *GSA Today*, *11*, 4–9.

Kay, S. M., and C. Mpodozis (2002), Magmatism as a probe to the Neogene shallowing of the Nazca plate beneath the modern Chilean flat-slab, *J. South. Am. Earth Sci.*, *15*, 39–57, doi:10.1016/S0895-9811(02)00005-6.

Kendrick, E., B. A. Brooks, M. Bevis, R. Smalley Jr., E. Lauria, M. Araujo, and H. Parra (2006), Active orogeny of the south-central Andes studied with GPS geodesy, *Rev. Asoc. Geol. Argent.*, *61*, 555–566.

Kirby, E., P. W. Reiners, M. A. Krol, K. X. Whipple, K. V. Hodges, K. A. Farley, W. Tang, and Z. Chen (2002), Late Cenozoic evolution of the eastern margin of the Tibetan Plateau: Inferences from $^{40}Ar/^{39}Ar$ and (U-Th)/He thermochronology, *Tectonics*, *21*(1), 1001, doi:10.1029/2000TC001246.

Kraemer, P. E., A. Tauber, C. Schmidt, and G. Ramé (1993), Analisis cinemático de la "Falla de Nono." Evidencias de actividad neotectónica. Valle de San Alberto, Provincia de Córdoba, paper presented at XII Congreso Geológico Argentino y II Congreso de Exploracíon de Hidrocarburos, Valle de San Alberto, Argentina, Actas TIII.

Langston, C. A. (1979), Structure under Mount Rainier, Washington, inferred from teleseismic body waves, *J. Geophys. Res.*, *84*, 4749–4762.

Lencinas, A., and A. Timonieri (1968), Algunas características estructurales del Valle de Punilla-Córdoba, *Actas Terceras J. Geol. Argent.*, *1*, 195–207.

Linares, E., A. J., Timonieri, and R. Pascual (1960), La edad de los sedimentos terciarios del Valle de Punilla Provincia de Córdoba y la presencia de *Eohyrax Rusticus* Ameghino en los mismos, *Rev. Asoc. Geol. Argent.*, *15*, 3–4, 191–210.

Löbens, S., F. A. Bense, K. Wemmer, I. Dunkl, C. H. Costa, P. Layer, and S. Siegesmund (2010), Exhumation and uplift of the Sierras Pampeanas: Preliminary implications from K–Ar fault gouge dating and low-T thermochronology in the Sierra de Comechingones (Argentina), *Int. J. Earth Sci.*, *100*, 671–694.

Martino, R. D. (2003), Las fajas de deformación dúctil de las Sierras Pampeanas de Córdoba: Una reseña general, *Rev. Asoc. Geol. Argent.*, *58*, 549–571.

Martino, R. D., P. Kraemer, M. Escayola, M. Giambastiani, and M. Arnosio (1995), Transecta de las Sierras Pampeanas de Córdoba a los 32°S, *Rev. Asoc. Geol. Argent.*, *50*, 60–77.

Massabie, A., A. Sanguinetti, G. Lo Forte, and M. Cegarra (2003), La actividad neotectónica en la sierra Baja de San Marcos-Cruz del Eje, flanco occidental de las Sierras Pampeanas Orientales, *Rev. Asoc. Geol. Argent.*, *58*, 653–663.

Mingorance, F. (1991), Análisis y evaluación del tectonismo reciente asociado a la Falla Sampacho, Provincia de Córdoba, Argentina central, *Rev. Geofis.*, *35*, 13–39.

Pankhurst, R. J., C. W. Rapela, J. Saavedra, E. Baldo, J. Dahlquist, I. Pascua, and C. M. Fanning, (1998), The Famatinian magmatic arc in the central Sierras Pampeanas, in *The Proto-Andean Margin of South America*, edited by R. J. Pankhurst and C. W. Rapela, *Geol. Soc. Spec. Publ.*, *142*, 343-367.

Perarnau, M., H. Gilbert, P. Alvarado, R. Martino, and M. Anderson (2012), Crustal structure of the Eastern Sierras Pampeanas of Argentina using high frequency local receiver functions, *Tectonophysics*, *580*, 208–217, doi:10.1016/j.tecto.2012.09.021.

Phinney, R. A. (1964), Structure of the Earth's crust from spectral behavior of long-period body waves, *J. Geophys. Res.*, *69*, 2997–3017.

Rahl, J. M., P. W. Reiners, I. H. Campbell, S. Nicolescu, and C. M. Allen (2003), Combined single-grain (U-Th)/He and U/Pb dating of detrital zircons from the Navajo Sandstone, Utah, *Geology*, *31*, 761–64.

Ramos, V. A. (2009), Anatomy and global context of the Andes: Main geologic features and the Andean orogenic cycle, in *Backbone of the Americas: Shallow Subduction, Plateau Uplift, and Ridge and Terrane Collision*, edited by S. M. Kay, V. A. Ramos, and W. R. Dickinson, *Mem. Geol. Soc. Am.*, *204*, 31-65.

Ramos, V. A., and A. Aleman (2000), Tectonic evolution of the Andes, in *Tectonic Evolution of South America Int. Geol. Congr. (31st), Río de Janeiro*, edited by U. G. Cordani, et al., pp. 635–685, Rio de Janeiro, Brazil.

Ramos, V. A., F. Munizaga, and S. M. Kay (1991), El magmatismo cenozoico a los 33ºS de latitud: Geocronología y relaciones tectónicas. VI Congreso Geológico Chileno, Vina del Mar, Chile,: Actas 1, pp. 892–896.

Ramos, V. A., E. O. Cristallini, and D. J. Perez (2002), The Pampean flat-slab of the Central Andes, *J. South Am. Earth Sci.*, *15*, 59–78.

Ramos, V. A., T. Zapata, E. O. Cristallini, and A. Introcaso (2004), The Andean thrust system—Latitudinal variations in structural styles and orogenic shortening, in *Thrust Tectonics and Hydrocarbon Systems*, edited by K. R. McClay, *AAPG Mem.*, *82*, 30-50.

Rapela, C. W., R. J. Pankhurst, C. Casquet, E. Baldo, J. Saavedra, and C. Galindo (1998), Early evolution of the Proto-Andean margin of South America, *Geology*, *26*, 707–710.

Rapela, C. W., R. J. Pankhurst, C. Casquet, C. M. Fanning, E. G. Baldo, J. M. González-Casado, C. Galindo, and J. Dahlquist (2007), The Río de la Plata craton and the assembly of SW Gondwana, *Earth Sci. Rev.*, *83*, 49–82.

Reiners, P. W., T. L. Spell, S. Nicolescu, and K. A. Zanetti (2004), Zircon (U-Th)/He thermochronometry: He diffusion and comparison with 40Ar/39Ar dating, *Geochim. Cosmochim. Acta*, *68*(8), 1857–1887.

Richardson, T. (2011), A geophysical and geologic analysis of the development, structure, and activity of the eastern Sierras Pampeanas, Argentina, M. S. thesis, Dep. of Earth, Atmos., and Planet. Sci., Purdue Univ., West Lafayette, Indiana.

Richardson, T., H. Gilbert, M. Anderson, K. D. Ridgway (2012), Seismicity within the actively deforming Eastern Sierras Pampeanas, Argentina, *Geophys. J. Int.*, *188*, 408–420, doi:10.1111/j.1365-246X.2011.05283.x.

Sagripanti, G. L., and D. Villalba (2009), Paleosismicidad y estimación del intervalo de recurrencia de fuertes terremotos asociados a fallas de intraplaca a la latitud 33ºS, falla Las Lagunas, Sampacho, Córdoba, *Rev. Asoc. Geol. Argent.*, *65*, 417–428.

Sagripanti, G. L., D. Origlia, and O. Campanella (1998), Historic and present seismology of the Sampacho area, Córdoba Province, Argentina, *Environ. Eng. Geosci.*, *IV*, 270–275.

Schmidt, C. J., R. A. Astini, C. H. Costa, C. E. Gardini, and P. E. Kraemer (1995), Cretaceous rifting, alluvial fan sedimentation, and neogene inversion, Southern Sierras Pampeanas, Argentina, in *Petroleum Basins of South America*, edited by A. J. Tankard, R. Suarez, and H. J. Welsink, *AAPG Mem.*, *62*, 341-358.

Schuster, D. L., R. M. Flowers, and K. A. Farley (2006), The influence of natural radiation damage on helium diffusion kinetics in apatite, *Earth Planet. Sci. Lett.*, *249*, 148–161.

Snyder, D. B., V. A. Ramos, and R. W. Allmendinger (1990), Thick-skinned deformation observed on deep seismic reflection profiles in western Argentina, *Tectonics*, *9*, 773–788.

Stern, C. R. (2004), Active Andean volcanism: its geologic and tectonic setting, *Rev. Geol. Chile*, *31*, 161–206.

Uliana, M. A., K. T. Biddle, and J. Cerdan (1989), Mesozoic extension and the formation of Argentine sedimentary basins, in *Extensional Tectonics and the Stratigraphy of the North Atlantic Margins*, edited by A. J. Tankard and H. R. Balkwill, *AAPG Mem.*, *46*, 599-614.

Urbina, N., P. Sruoga, and L. Malvicini (1997), Late Tertiary gold-bearing volcanic belt in the Sierras Pampeanas of San Luis, Argentina, *Int. Geol. Rev.*, *39*, 287–306.

Vigny, C., A. Rudloff, J. Ruegg, R. Madariaga, J. Campos, and M. Alvarez (2009), Upper plate deformation measured by GPS in the Coquimbo Gap, Chile, *Phys. Earth Planet. Inter.*, *175*, 86–95.

Warnock, A. C., P. K. Zeitler, R. A. Wolf, and S. C. Bergman (1997), An evaluation of low-temperature apatite U-Th/He thermochronometry, *Geochim. Cosmochim. Acta*, *61*, 5371–77.

Yáñez, G., and J. Cembrano (2004), Role of viscous plate coupling in the late Tertiary Andean tectonics, *J. Geophys. Res.*, *109*, B02407, doi:10.1029/2003JB002494.

Yañez, G., J. Cembrano, M. Pardo, C. Ranero, and D. Selles (2002), The Challenger-Juan Fernandez-Maipo major tectonic transition of the Nazca-Andean subduction system at 33-34°S: Geodynamic evidence and implications, *J. South Am. Earth Sci.*, *15*, 23–38.

Zapata, T. R., and R. W. Allmendinger (1996), Thrust-front zone of the Precodillera, Argentina: A thick-skinned triangle zone, *AAPG Bull.*, *80*, 359–381.